C.P. No. 1163

C.P. No. 1163

MINISTRY OF AVIATION SUPPLY

AERONAUTICAL RESEARCH COUNCIL

CURRENT PAPERS

Low-Speed Wind-Tunnel Tests on a Family of Cambered Wings of Mild Gothic Planform of Aspect Ratio 1.4

by

P. J. Butterworth

Aerodynamics Dept., R.A.E., Farnborough

LONDON: HER MAJESTY'S STATIONERY OFFICE

1971

PRICE 55p NET

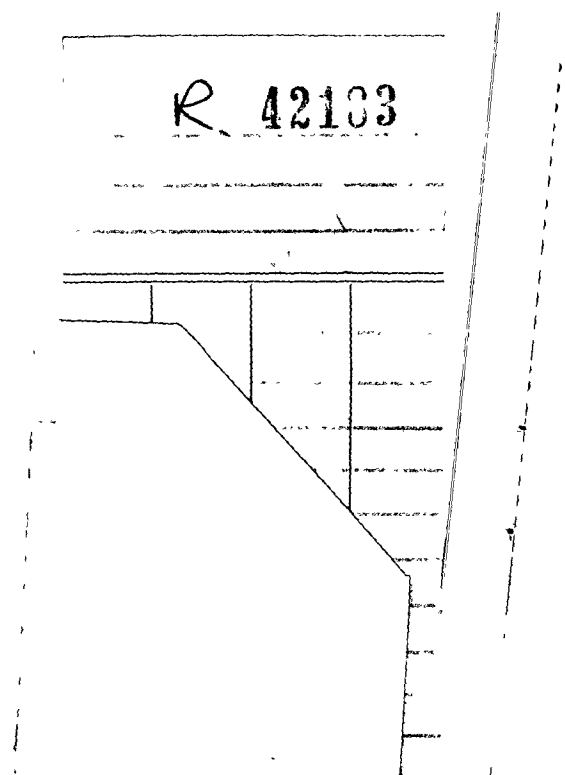

UDC 533.693.3 : 533.6.043.1 : 533.6.013.12 : 533.6.013.13 : 533.6.013.152

C.P. No.1163*
October 1970

LOW-SPEED WIND-TUNNEL TESTS ON A FAMILY OF CAMBERED WINGS OF MILD GOTHIC PLANFORM OF ASPECT RATIO 1.4

by

P. J. Butterworth

Aerodynamics Department, RAE, Farnborough

SUMMARY

The longitudinal characteristics of a family of one symmetrical and two cambered mild gothic wings of aspect ratio 1.4 and thickness-to-chord ratio of 0.09 were investigated and the results are presented with analysis. The two cambered wings were designed to have attached leading edge flow at lift coefficients of 0.1 and 0.2 respectively, at a specified angle of incidence. The force measurements and flow visualisation show that the design criteria have in fact been satisfied though additional inboard shoulder separations near the apex were observed under certain conditions.

---

* Replaces RAE Technical Report 70185 - ARC 32686.

CONTENTS

1 INTRODUCTION

Three mild gothic wings were tested in the 4ft × 3ft low-speed wind tunnel at RAE Farnborough. Of the three wings, one was symmetrical and the other two were cambered both chordwise and spanwise in an attempt to reduce drag at lift coefficients appropriate to take-off, without penalising cruise values.

The two cambered wings were designed using a linear theory[1] to give attached flows at specified values of C_L. Thus this series of tests has a two-fold purpose. Firstly, do the cambered wings fulfil their design criteria and secondly, how does their performance compare with that of the symmetric wing?

The current tests were run at both 30.5 m/sec and 61 m/sec to examine Reynolds number effect. Lift, drag and pitching moment were measured over a range of angles of incidence and for visual assessment, flow visualisation using a suspension of lamp-black in paraffin was examined and photographed.

2 MODEL AND TEST DETAILS

For convenience, the three models will be referred to as A, B and C, where model A is the symmetric wing which is used as a datum in the analysis of the results and models B and C are the cambered wings.

The three wings were designed with the starboard leading edge given by:

$$y = s(x) = 0.047\,625\,(5(x/c) - (x/c)^5)_m$$

and a straight trailing edge (see Fig.1). For the two wings cambered for attached flow, a load distribution is specified thus defining C_L and the position of the centre of pressure. Nothing is assumed about the flow for incidences above the attachment condition. Consistent with the geometric parameters, a computer programme then calculates the co-ordinates of the camber surface and these co-ordinates also specify the angle of incidence for attached flow. That is, the camber surface is defined in x,y,z co-ordinates, these being taken in the usual senses. The apex lies on the z-axis and the trailing edge in the xy plane (along $x = 0.4717$ m). The angle between the xy plane and the plane defined by the trailing edge and apex is the incidence at which attached flow is expected. For models B and C, the relevant design parameters are given in the table below:

	$(C_L)_{DES}$	α_{DES}	$\frac{x_{c.p.}}{c}$
B	0.1	5.32	0.533
C	0.2	10.55	0.533

It is evident from the above description, that this method of design gives A, B and C slightly different values of centre-line chord and plan area (and hence aspect ratio). (See Table 1).

There exists some choice in how the thickness distribution can be added to a camber surface. In this case, spanwise cross-sections of the camber surfaces (normal to the xy plane) were taken, and the thickness added normally to these lines. The thickness distribution for all three models was the same. Typical spanwise sections are shown in Fig.2.

For the flow visualisation tests, the models were mounted on a sting and a suspension of lamp-black in paraffin was used at wind speeds of 30.5, 48.8 and 61 m/sec. Early tests showed that it was impossible to reach the highest wind speed before the paraffin evaporated and for this reason, most of these tests were run at 30.5 m/sec. The photographic results of these tests are discussed in greater detail in the next section.

The models were hung on a wire rig for the force measurements but unfortunately, this led to some restriction on the range of angles of incidence especially for model C when considerable negative lift was encountered for small negative incidences. In fact, for this model, the range of incidence was restricted to $-1^{o} \leqslant \alpha \leqslant 25^{o}$ (before correction). The raw data was reduced to coefficient form taking account of tunnel blockage and constraints and the contributions of the wire rig to drag and pitching moment. For symmetric wings, it is standard practice to make small corrections to α and C_m to ensure that the C_L vs. α and C_m vs. α graphs pass through the origin. This practice eliminates experimental and model irregularities. However, for the two cambered wings no such corrections to α and C_m can be made without pre-judging the effectiveness of the design theory. For this reason it was thought necessary to test the symmetric wing both ways up to investigate the effect of the rig on the wing in some detail. Lift and pitching moment were unaffected by this exercise though the inverted wing showed slightly more drag than when normal. This can be accounted for by the main cleats which did not fit into the model as cleanly when inverted. Therefore, for all three models no corrections have been applied to α and C_m.

The force tests were run under transition free conditions at wind speeds of 30.5 and 61 m/sec corresponding to Reynolds numbers of 1×10^6 and 2×10^6 based on the centre-line chord of model A. Only the results of the 61 m/sec runs are presented in Table 2 since the effect of Reynolds number over this limited range are negligible - see Figs.3 and 4. Attempts were made to suppress flow separations from the upper surface of wings B and C, see section 3, by applying roughness in the form of small glass balls near the leading edge but there was no noticeable effect on the oil flow patterns and for this reason, the force measurements on the models were made without trying to fix transition. In order to investigate the properties of wing B at higher Reynolds numbers, a larger model with a 1.276 m (4.167 ft) centre-line chord is being made with facilities for obtaining surface static pressures.

3 FLOW VISUALISATION

For the flow visualisation tests, the models were mounted on a rear sting which was bolted to the underside of the model thus leaving the upper surface clean, and observations were made at angles of incidence up to 25° on all three wings. A number of flow patterns on the three models were photographed, the majority being of the upper surface at a wind speed of 30.5 m/sec. Two of the photographs were of patterns on the lower surfaces of the two cambered wings 5° below their respective attachment incidences and another two were of patterns obtained at a wind speed of 48.8 m/sec to see if there were any visible effects of changing the Reynolds number.

Fig.5 shows that at the design incidence for wing C, $\alpha = 10.55^\circ$, the flow is attached at the leading edge though it does separate further inboard. Full views of the flows over wings B and C at their respective attachment incidences are shown in Fig.6 and for each model, there is attached flow at the leading edges for the design incidence. It was in an attempt to prevent the shoulder separations observed near the apex that strips of roughness were applied near the leading edges of wing C. At a Reynolds number of 1×10^6 based on centre-line chord, the strips were ineffective but it is hoped that the nature of this flow will be more thoroughly investigated and understood using the larger pressure plotting model of wing B that is presently under construction.

Another important aspect of the flow observations is the position of the primary vortices above the wings. For a given angle above the attachment condition, these vortices move out towards the leading edge as the camber is increased. Also, as incidence is increased, the vortices move inboard as

shown in Fig.7. This figure shows the position of the point of inflection on the surface pattern under the primary vortex plotted against incidence above the attachment condition and quantitatively illustrates the two points mentioned above. The measurements necessary for Fig.7 were taken from photographs such as those shown in Figs.8 and 9.

These two figures raise another point: the apparent existence of vortices close to the centre-line on models B and C. Figs.5 and 6 show the shoulder separations that exist on these two models at their design incidences and Figs.8 and 9 show the separations persisting at higher incidences. It seems likely that due to the upper surface curvature, the flow separates near the apex and this separated flow is then carried downstream. The area affected by this flow near the centre-line decreases with increasing incidence but increases with camber. The change in Reynolds number from 1×10^6 to 1.6×10^6 based on centre-line chord produced no change in the patterns apart from increasing the definition.

4 FORCE MEASUREMENTS

The results of the force measurements at V = 61 m/sec are given in Table 2 and plotted in Figs.10 to 20.

4.1 Lift and drag

Fig.10 shows C_L plotted against incidence, α. If we denote the lift coefficient at the design attachment incidence (α_{DES}) by $\left(C_L\right)_{\alpha_{DES}}$ for the two cambered wings, as in Fig.11, these values can be used to superimpose the attached flow conditions for all three wings. The values of $\left(C_L\right)_{\alpha_{DES}}$ for wings B and C are 0.103 and 0.194 respectively (departures from the theoretical design coefficients of only +3% and -3% respectively). It can be seen from this figure that at any given angle above the attached flow condition, the value of $[C_L - \left(C_L\right)_{\alpha_{DES}}]$ is little affected by camber and in fact at higher values of $[\alpha - \alpha_{DES}]$, wing C lies up to only 8% below wing A and 4% below wing B. Considering that in the design of the cambered wings no assumptions were made about the $C_L \sim \alpha$ relationship above the attachment incidence, this is quite gratifying.

When examining the drag polars of a family of cambered wings (as plotted in Fig.12) we need to consider the ways in which we can define the induced drag. Warren[2] investigated the existence of a parabolic envelope to the drag polars of a family of cambered wings whose surfaces are scaled versions of one another. For a symmetric wing, the induced drag factor K is defined by:

$$K = \pi A \frac{\left(C_D - C_{D_o}\right)}{C_L^2} \tag{1}$$

where C_{D_o} is the drag coefficient at zero lift. This may be written:

$$C_D = C_{D_o} + \frac{K}{\pi A} C_L^2 \quad . \tag{2}$$

The analogous definition for a cambered wing is:

$$C_D = C_{D_m} + X\left(C_L - C_{L_m}\right)^2 \tag{3}$$

where X is assumed constant for the family of cambered wings and $\left(C_{L_m}, C_{D_m}\right)$ is the minimum point of the $C_D \sim C_L$ curve of the wing in question.

Alternatively for a cambered wing we may write:

$$C_D = C_{D_o} + t\, C_L^2 \tag{4}$$

where C_{D_o} is the drag coefficient at zero lift of the symmetrical member of the camber family and t is a function of C_L.

Therefore, to find the envelope of the form:

$$C_{D_e} = C_{D_o} + k\, C_L^2$$

to equations (2) and (4), we only need to minimise t with respect to C_L in (4). For example consider C_D plotted against C_L^2 for a cambered wing and join $\left(0, C_{D_o}\right)$ to any point on that curve. The envelope is defined by the point at which this line touches the curve, which is when t is a minimum. (Call this value t_{min}.)

Therefore the envelope is given by:

$$C_{D_e} = C_{D_o} + t_{min}\, C_L^2 \quad .$$

From Fig.13a, it can be seen that B and C have minimum values of K_1 corresponding to $t_{min} = 0.31$ at $C_L = 0.28$ and 0.42 respectively, i.e. for this family of wings, we do have a parabolic envelope of the drag polars and its equation is:

$$C_{D_e} = 0.0072 + 0.31\, C_L^2$$

defining a polar which is compared with the measured coefficients in Fig.12.

In the above analysis, it is assumed that for the unique determination of the envelope to the drag polars, X is a constant for the family of cambered wings. The numerical evaluation of C_{D_o}, C_{D_m} and C_{L_m}, necessary for the determination of X, is dealt with in the Appendix and the results are presented in Figs.13b and 14. Fig.13b shows $K_2 (= \pi A\, X)$ as a function of $\left(C_L - C_{L_m}\right)$. For wings A and B this figure and more particularly Fig.14 show that X has a mean value of 0.364 in the region $\left(C_L - C_{L_m}\right) < 0.3$ though wing C takes a higher value. Despite this the drag polar for wing C touches the envelope of the drag polars of wings A and B and we can use the results of the present tests to postulate, for the lower lift coefficients, a cambered wing of this family such that its drag at a specified $C_L \left(C_{L_e} \text{ say}\right)$ is $0.0072 + 0.31\left(C_{L_e}\right)^2$ - a minimum for the family. To do this, we need to know the relationship between the design attachment value of C_L and the value of C_L at which the drag polar touches the envelope. This relationship can be obtained from the results of these tests and it is plotted in Fig.15. An example below this figure shows that a member of this camber family could be designed to reduce the drag at say $C_L = 0.15$ by at least 4% compared to any of the wings tested.

At the higher lift coefficients appropriate to take-off and landing, the results indicate that it is unlikely that the low values of the minimum polar could be realised by a further extension of the present camber series. Because of the increased value of X on wing C compared with A and B, the reductions in drag achieved by increasing the camber become less marked. Thus at $C_L = 0.5$, the drag of wing B is nearly 9% less than wing A but doubling the design C_L yields only another 4% reduction and at still higher C_L's, the drags of B and C become even closer.

Although the analysis of the normal force coefficient is not one of the main factors of this Report, it is included briefly for completeness. Kirkpatrick[3] and Kirby[4] have separated C_N into its linear and non-linear components:

$$C_N = C_{N_{linear}} + C_{N_{non\text{-}linear}} = a\,\alpha + C_{N_{n.\ell.}}$$

where a is the intercept on the C_N/α axis of a plot of C_N/α vs. α. For cambered wings this becomes:

$$C_N = \left(C_N\right)_{\alpha_{DES}} + a(\alpha - \alpha_{DES}) + C_{N_{n.\ell.}}$$

Thus, for a realistic comparison of the three wings and the determination of a in the above equations, a generalised form of C_N/α is plotted in Fig.16. For the two cambered wings, $(C_N - \left(C_N\right)_{\alpha_{DES}})/(\alpha - \alpha_{DES})$ is plotted against α for incidences above and below α_{DES}. The first point of this graph is the different values of a for the three wings: 1.620, 1.400 and 1.542 for A, B and C respectively. Remembering the agreement in $[C_L - \left(C_L\right)_{\alpha_{DES}}]$ vs. $[\alpha - \alpha_{DES}]$ curves in Fig.11, this seems surprising, but closer inspection of Figs.10 and 11 shows that at attachment, the gradients of the C_L vs. α curves for the three wings do differ in this manner.

The second point of interest is the occurrence of vortex breakdown on wings A and B. This is shown on the C_N/α graph by a point of inflection in the region $15^\circ \leqslant \alpha \leqslant 20^\circ$. No such characteristic is evident for wing C. Examination of pitching moment curves (and hence the position of the aerodynamic centre) in the next section confirms these observations.

4.2 Pitching moment

Figs.17 and 18 show the pitching moment plotted against incidence and lift respectively. These moments are referred to a centre of gravity at 0.54 c from the wing apex. All three wings demonstrate the characteristic loss in stability near their respective design conditions and for models A and B in the region of $C_L = 0.5$, there is a further loss of stability which must be due to vortex breakdown as mentioned in the previous subsection. No such tendencies are shown by wing C which again confirms the observations from the C_N/α graphs.

The position of the centre of pressure is shown in Fig.19 for all three wings. One of the design parameters for the two cambered wings is that at attachment, the centre of pressure is at 0.533 c from the wing apex. These wind-tunnel tests have shown that it is at 0.513 c and 0.50 c for B and C respectively. This is an error of 2% and 3.3% of the centre-line chord and

considering the large cambers involved, it would not be surprising if the assumptions of linear theory have been violated. For wing A, the centre of pressure moves between 0.538 c and 0.558 c but for $C_L > 0.7$ it is constant at 0.553 c. As C_L increases, so all three curves of centre of pressure vs. lift converge to this value.

The aerodynamic centre vs. lift curves in Fig.20 are derived from C_m vs. C_N curves and because of the breakdown of the vortices, wings A and B demonstrate a sudden forward movement of $x_{a.c.}$ near $C_L = 0.5$. On all three wings an aft movement of the aerodynamic centre as C_L rises above the attached flow value results from the loss of stability mentioned earlier.

5 CONCLUSIONS

There can be little doubt that the design theory for the two cambered wings has succeeded in giving attached flow at the specified incidence and the force measurements show good agreement with the design conditions. The two cambered wings have lower drag than the symmetric one over quite a wide range of lift coefficient, though at the lower end of this range, there is some uncertainty due to the low Reynolds number at which these tests were run. The existence of an envelope to the drag polars has been proved and its use in further reduction of drag at a specific value of lift coefficient (applicable to cruise) has been shown. However, it is unlikely that much further reduction in drag at lift coefficients applicable to take-off and landing can be achieved with the present family of cambered wings as it appears that the assumptions of linear theory in the design have already been violated; for example at $C_L = 0.5$ wing B reduces the drag of wing A by nearly 9% but wing C only reduces it by a further 4%. Use of the envelope curve shows that these reductions in drag at lift coefficients applicable to take-off conditions are achieved with little penalty to the lower lift coefficients which are more applicable to cruise.

For all three models, the centre of pressure moves aft with increasing incidence and for each of the cambered wings the positive increment of pitching moment coefficient at $\alpha = 0^o$ ensures that a stable, trimmed condition exists at some lift coefficient dependent on the position of the centre of gravity.

It appears that the leading edge vortices above wings A and B break down as the lift coefficient increases to 0.5 though no such tendency is evident for wing C. It is unlikely that the two cambered wings have vortices of any strength near the centre-line as, if anything, their lift at a given angle above

the designed attachment incidence is lower than that of the symmetric wing. Probably, the separated flows as seen in Figs.8 and 9 are caused by shoulder separations near the apex and the weak vortices are then carried downstream.

It is hoped that some of the questions raised by this preliminary investigation into the value of the linear theory used, will be satisfactorily answered by the results of the future tests on the larger pressure plotting models of wings A and B that are under construction.

Appendix

THE DETERMINATION OF C_{D_o}, C_{D_m} AND C_{L_m}

To find the envelope of the drag polars of the three wings, we need to know the values of the constants C_{D_o}, C_{D_m} and C_{L_m}. For a symmetric wing, to determine C_{D_o}, C_D is plotted against C_L^2 for positive and negative values of C_L. For $0 < C_L < 0.3$, these points lie approximately on a straight line* and C_{D_o} is defined by the intercept of this line and the C_D axis. For wing A, C_{D_o} takes the value 0.0072 (see Fig.14).

Having evaluated C_{D_o}, it is possible to deduce the equation of the envelope of the drag polars, but this assumes that X as defined by:

$$C_D = C_{D_m} + X\left(C_L - C_{L_m}\right)^2$$

is a constant for the family of cambered wings. To see whether or not it is a constant requires the evaluation of C_{D_m} and C_{L_m} for each of the cambered wings, but doing this to any degree of accuracy poses a problem for which the author used the following iterative process based on the method of evaluating C_{D_o} for a symmetric wing:

From a suitably scaled C_D vs. C_L graph, choose C_L such that C_D appears to be a minimum. Call this value of C_L, $\left[C_L\right]_1$ and plot C_D against $(C_L - \left[C_L\right]_1)^2$. Three situations can arise:

(i) all points lie on or close to one straight line;

(ii) positive values of $C_L - \left[C_L\right]_1$ lie on one straight line and negative values on another and these two lines intersect on the C_D axis;

(iii) one line of positive points and one of negative points not intersecting on the C_D axis.

Of these alternatives, only the first two are acceptable (see Fig.14). If situation (iii) arises, a new value of $\left[C_L\right]_1$ is needed such that when repeating the plotting an acceptable form results. The last value of

---

* Due to the presence of the laminar drag bucket, the points with very low values of C_L tend to lie below this line.

C_L, $[C_L]_n$ say, is then C_{L_m} and the intercept on the C_D axis is C_{D_m}. These values can then be used in the definition of X (or K_2 as in Fig.13b).

Two points should be noticed with regard to the three situations indicated above. Firstly, (ii) is an acceptable form since it merely indicates that the inverted wing is different from the normal wing, though its drag polar is not of the same form as the symmetric wing (i.e. X is not constant for the family of cambered wings). Secondly, the lines of points in (iii) need not be straight.

Table 1

MODEL DETAILS

Parameter \ Model	A	B	C
Wing area	0.10484 m^2	0.10535 m^2	0.10647 m^2
Wing chord	0.4717 m	0.4740 m	0.4791 m
Aspect ratio	1.385	1.378	1.363
max t/c	9.02%	8.94%	8.72%
$x_{c.a.}/c$	0.6531	0.6531	0.6531
P.M. centre/c	0.54	0.54	0.54
Slenderness ratio	0.404	0.402	0.398
α_{DES}	0	5.32^o	10.55^o
$\left(C_L\right)_{DES}$	0	0.1	0.2
$\left(C_L\right)_{\alpha_{DES}}$	0.0	0.103	0.194
C_{D_m}	0.0072	0.0101	0.0149
C_{L_m}	0.0	0.038	0.077

Thickness distribution given by: $z = \pm B(x)\ (1 - y^2/s^2(x))$

where $s(x) = 0.047\ 625\ (5(x/c) - (x/c)^5)$ is the starboard leading edge and $B(x) = 0.4717\ (x/c)\ (1 - x/c)\ (0.29224 - 0.68199\ (x/c) + 1.60782\ (x/c)^2 - 1.72866\ (x/c)^3 + 0.69079\ (x/c)^5)$ is the centre-line thickness distribution (in metres).

Table 2

SYMMETRICAL MILD GOTHIC WING V = 61 m/sec (200 ft/sec)

α^o	C_L	C_D	C_N	C_A	$C_m(0.54)$	C_N/α	K_1	K_2	$\frac{x_{c.p.}}{c}$	$\frac{x_{a.c.}}{c}$
-4.77	-0.1565	0.01664	-0.1574	0.0036	0.00203	1.890				
-4.26	-0.1431	0.01542	-0.1438	0.0048	0.00161	1.935				
-3.74	-0.1195	0.01280	-0.1201	0.0050	0.00129	1.841				
-3.22	-0.1020	0.01144	-0.1025	0.0057	0.00065	1.823	$K_1 = K_2$ for this wing			
-2.70	-0.0802	0.00964	-0.0805	0.0059	0.00032	1.708				
-2.19	-0.0642	0.00863	-0.0645	0.0062	0.00044	1.690				
-1.67	-0.0492	0.00776	-0.0495	0.0063	0.00028	1.693				
-1.16	-0.0357	0.00677	-0.0358	0.0060	0.00028	1.766				
-0.65	-0.0211	0.00610	-0.0211	0.0059	0.00071	1.868				
-0.13	-0.0047	0.00589	-0.0047	0.0059	0.0	1.995				
0.38	0.0110	0.00588	0.0110	0.0058	0.0	1.661			0.5405	0.541
0.89	0.0267	0.00635	0.0268	0.0059	-0.00025	1.716			0.5430	0.543
1.41	0.0452	0.00751	0.0454	0.0064	-0.00007	1.843	0.553		0.5440	0.545
1.92	0.0589	0.00843	0.0592	0.0065	0.0	1.763	1.479		0.5450	0.547
2.44	0.0752	0.00933	0.0756	0.0061	-0.00038	1.777	1.594		0.5448	0.548
2.95	0.0934	0.01048	0.0938	0.0057	-0.00074	1.819	1.610		0.5467	0.550
3.47	0.1097	0.01173	0.1102	0.0051	-0.00088	1.821	1.617		0.5482	0.554
3.98	0.1272	0.01331	0.1278	0.0044	-0.00108	1.838	1.629		0.5488	0.556
4.50	0.1455	0.01511	0.1462	0.0037	-0.00165	1.862	1.615		0.5508	0.559
5.02	0.1704	0.01809	0.1714	0.0031	-0.00234	1.955	1.624		0.5534	0.560
5.54	0.1881	0.02023	0.1892	0.0020	-0.00269	1.958	1.600		0.5541	0.560
6.58	0.2294	0.02654	0.2310	0.0001	-0.00354	2.013	1.594		0.5553	0.560
7.61	0.2689	0.03353	0.2710	-0.0024	-0.00434	2.040	1.581		0.5562	0.560
8.65	0.3110	0.04230	0.3138	-0.0049	-0.00521	2.079	1.577		0.5570	0.560
9.74	0.3623	0.05463	0.3663	-0.0075	-0.00624	2.154	1.570		0.5575	0.559
10.74	0.4077	0.06707	0.4131	-0.0101	-0.00730	2.205	1.566		0.5582	0.558
11.77	0.4508	0.08028	0.4577	-0.0134	-0.00807	2.228	1.563		0.5582	0.557
12.82	0.4969	0.09601	0.5059	-0.0166	-0.00848	2.262	1.564		0.5574	0.553
13.86	0.5457	0.11487	0.5573	-0.0192	-0.00811	2.304	1.573		0.5552	0.509
14.89	0.5848	0.13286	0.5993	-0.0219	-0.00664	2.305	1.598		0.5520	0.518
15.93	0.6256	0.15247	0.6434	-0.0251	-0.00663	2.314	1.614		0.5510	0.543
16.97	0.6702	0.17599	0.6924	-0.0273	-0.00710	2.338	1.635		0.5510	0.553
18.01	0.7162	0.20157	0.7434	-0.0298	-0.00796	2.365	1.648		0.5515	0.558
19.06	0.7624	0.22887	0.7953	-0.0326	-0.00854	2.392	1.659		0.5519	0.560
20.10	0.8098	0.25654	0.8487	-0.0374	-0.00963	2.420	1.654		0.5522	0.560
21.15	0.8679	0.29622	0.9163	-0.0369	-0.01132	2.482	1.669		0.5536	0.560
22.20	0.9169	0.33206	0.9744	-0.0389	-0.01223	2.516	1.681		0.5535	0.560
23.24	0.9650	0.36741	1.0317	-0.0432	-0.01278	2.544	1.683		0.5536	0.559
24.28	1.0149	0.40889	1.0933	-0.0447	-0.01369	2.580	1.697		0.5536	
25.32	1.0539	0.44392	1.1425	-0.0494	-0.01419	2.585	1.711		0.5535	
26.36	1.1011	0.48785	1.2032	-0.0519	-0.01497	2.615	1.725		0.5536	

Table 2 (Contd)

CAMBERED MILD GOTHIC WING: $C_L = 0.1$ V = 61 m/sec (200 ft/sec)

α^o	C_L	C_D	C_N	C_A	$C_m(0.54)$	C_N/α	K_1	K_2	$\frac{x_{c.p.}}{c}$	$\frac{x_{a.c.}}{c}$
-2.82	-0.2019	0.03087	-0.2031	0.0209	0.00885	2.139				
-1.77	-0.1549	0.02387	-0.1556	0.0191	0.00782	2.071				
-1.25	-0.1318	0.02090	-0.1322	0.0180	0.00715	2.031				
-0.73	-0.1084	0.01819	-0.1086	0.0168	0.00645	1.982				
-0.21	-0.0858	0.01589	-0.0858	0.0156	0.00591	1.932				
0.31	-0.0676	0.01439	-0.0675	0.0147	0.00553	1.923				
0.83	-0.0454	0.01281	-0.0452	0.0135	0.00474	1.861				
1.35	-0.0234	0.01161	-0.0232	0.0122	0.00431	1.787				
1.86	-0.0069	0.01091	-0.0066	0.0111	0.00396	1.776				
2.38	0.0136	0.01022	0.0140	0.0096	0.00330	1.687				
2.90	0.0274	0.00989	0.0279	0.0085	0.00326	1.721			0.4250	0.557
3.41	0.0463	0.00952	0.0467	0.0068	0.00288	1.616			0.4802	0.553
3.93	0.0615	0.00955	0.0620	0.0053	0.00286	1.637			0.4954	0.548
4.44	0.0782	0.00977	0.0787	0.0037	0.00260	1.419			0.5083	0.543
4.95	0.0911	0.00981	0.0916	0.0019	0.00284	1.375	1.361		0.5103	0.537
5.47	0.1079	0.01046	0.1084	0.0001	0.00286	2.831	1.212	0.318	0.5150	0.533
5.98	0.1202	0.01116	0.1207	-0.0014	0.00260	1.744	1.187	0.675	0.5151	0.525
7.01	0.1459	0.01451	0.1466	-0.0034	0.00389	1.561	1.486	1.646	0.5140	0.519
7.52	0.1601	0.01564	0.1608	-0.0054	0.00411	1.569	1.426	1.610	0.5153	0.529
8.04	0.1785	0.01760	0.1792	-0.0075	0.00390	1.656	1.412	1.648	0.5190	0.546
8.55	0.1924	0.01914	0.1932	-0.0097	0.00384	1.643	1.396	1.644	0.5208	0.550
9.07	0.2127	0.02154	0.2135	-0.0123	0.00351	1.725	1.371	1.624	0.5243	0.555
9.59	0.2327	0.02411	0.2335	-0.0150	0.00319	1.783	1.352	1.600	0.5270	0.558
10.11	0.2537	0.02723	0.2545	-0.0177	0.00253	1.840	1.348	1.595	0.5307	0.563
10.62	0.2698	0.02976	0.2707	-0.0205	0.00228	1.838	1.342	1.585	0.5322	0.568
11.14	0.2920	0.03358	0.2930	-0.0235	0.00116	1.894	1.339	1.576	0.5366	0.573
11.66	0.3093	0.03683	0.3103	-0.0264	0.00096	1.895	1.341	1.572	0.5375	0.573
12.18	0.3330	0.04179	0.3343	-0.0294	-0.00017	1.951	1.350	1.572	0.5418	0.569
12.70	0.3558	0.04672	0.3573	-0.0326	-0.00045	1.992	1.352	1.570	0.5447	0.568
13.74	0.3978	0.05728	0.4000	-0.0388	-0.00171	2.037	1.370	1.577	0.5469	0.564
14.78	0.4433	0.06993	0.4465	-0.0455	-0.00291	2.094	1.382	1.576	0.5480	0.560
15.82	0.4876	0.08407	0.4921	-0.0521	-0.00375	2.136	1.399	1.584	0.5473	0.556
16.86	0.5287	0.09940	0.5348	-0.0582	-0.00370	2.155	1.428	1.605	0.5473	0.542
17.90	0.5705	0.11762	0.5790	-0.0634	-0.00402	2.178	1.469	1.641	0.5473	0.554
18.94	0.6178	0.13889	0.6295	-0.0692	-0.00589	2.224	1.493	1.658	0.5497	0.569
19.99	0.6669	0.16227	0.6822	-0.0755	-0.00782	2.271	1.509	1.666	0.5518	0.575
21.04	0.7165	0.18747	0.7361	-0.0822	-0.00957	2.316	1.520	1.668	0.5533	0.573
22.09	0.7699	0.21683	0.7949	-0.0886	-0.01119	2.371	1.531	1.670	0.5544	0.570
23.13	0.8213	0.24868	0.8529	-0.0940	-0.01311	2.419	1.550	1.683	0.5556	0.567
24.18	0.8655	0.27773	0.9033	-0.1011	-0.01419	2.438	1.563	1.692	0.5560	0.566
25.22	0.9097	0.30859	0.9544	-0.1084	-0.01541	2.458	1.577	1.700	0.5564	0.564
26.27	0.9599	0.34741	1.0145	-0.1132	-0.01736	2.501	1.598	1.718	0.5573	0.562

Table 2 (Contd)

CAMBERED MILD GOTHIC WING: C_L = 0.2 V = 61 m/sec (200 ft/sec)

α^o	C_L	C_D	C_N	C_A	$C_m(0.54)$	C_N/α	K_1	K_2	$\frac{x_{c.p.}}{c}$	$\frac{x_{a.c.}}{c}$
-0.86	-0.2399	0.04774	-0.2405	0.0442	0.01414	2.182				
-0.33	-0.2086	0.04194	-0.2088	0.0407	0.01344	2.121				
0.19	-0.1911	0.03829	-0.1910	0.0389	0.01357	2.129				
0.71	-0.1741	0.03520	-0.1736	0.0373	0.01362	2.141				
1.23	-0.1501	0.03149	-0.1494	0.0347	0.01311	2.111				
1.75	-0.1256	0.02826	-0.1246	0.0321	0.01246	2.075				
2.27	-0.1081	0.02598	-0.1070	0.0302	0.01232	2.083				
2.79	-0.0840	0.02320	-0.0826	0.0273	0.01159	2.044				
3.31	-0.0660	0.02145	-0.0646	0.0252	0.01138	2.047				
3.83	-0.0430	0.01945	-0.0416	0.0223	0.01073	2.009				
4.35	-0.0198	0.01780	-0.0184	0.0192	0.01041	1.963				
4.87	-0.0043	0.01681	-0.0029	0.0171	0.01043	1.986				
5.39	0.0167	0.01570	0.0181	0.0141	0.01007	1.953				0.558
5.91	0.0374	0.01491	0.0387	0.0110	0.00991	1.918			0.2864	0.556
6.42	0.0581	0.01442	0.0593	0.0078	0.00921	1.869			0.3872	0.555
6.94	0.0770	0.01424	0.0782	0.0048	0.00924	1.838			0.4239	0.554
7.46	0.0929	0.01428	0.0938	0.0021	0.00904	1.858			0.4456	0.553
7.98	0.1120	0.01452	0.1129	-0.0012	0.00882	1.808			0.4638	0.553
8.49	0.1271	0.01498	0.1279	-0.0039	0.00859	1.839	2.062	0.137	0.4746	0.552
9.01	0.1459	0.01568	0.1465	-0.0073	0.00832	1.767	1.706	0.711	0.4849	0.551
9.52	0.1640	0.01612	0.1644	-0.0112	0.00804	1.647	1.421	0.688	0.4927	0.550
10.04	0.1791	0.01739	0.1793	-0.0141	0.00793	1.651	1.358	1.025	0.4973	0.549
10.55	0.1939	0.01893	0.1941	-0.0169	0.00796	-	1.336	1.260	0.5006	0.537
11.07	0.2085	0.02073	0.2086	-0.0197	0.00809	1.598	1.332	1.443	0.5026	0.531
11.58	0.2199	0.02293	0.2200	-0.0217	0.00873	1.441	1.393	1.694	0.5017	0.530
12.09	0.2377	0.02557	0.2378	-0.0248	0.00859	1.626	1.392	1.771	0.5051	0.532
12.61	0.2567	0.02833	0.2567	-0.0284	0.00827	1.741	1.373	1.781	0.5090	0.535
13.12	0.2692	0.03031	0.2690	-0.0316	0.00862	1.670	1.365	1.789	0.5091	0.537
13.64	0.2872	0.03308	0.2869	-0.0356	0.00868	1.721	1.343	1.762	0.5109	0.538
14.16	0.3054	0.03641	0.3050	-0.0394	0.00859	1.760	1.340	1.765	0.5129	0.541
14.67	0.3193	0.03912	0.3188	-0.0430	0.00864	1.734	1.340	1.767	0.5140	0.542
15.70	0.3538	0.04602	0.3531	-0.0515	0.00855	1.769	1.328	1.740	0.5167	0.545
16.74	0.3880	0.05377	0.3871	-0.0602	0.00824	1.787	1.323	1.722	0.5196	0.550
17.77	0.4284	0.06382	0.4274	-0.0700	0.00760	1.852	1.321	1.697	0.5262	0.556
18.81	0.4684	0.07517	0.4676	-0.0799	0.00681	1.897	1.327	1.685	0.5297	0.562
19.85	0.5087	0.08820	0.5084	-0.0898	0.00564	1.936	1.340	1.684	0.5331	0.566
20.89	0.5525	0.10372	0.5532	-0.1001	0.00423	1.990	1.353	1.683	0.5358	0.568
21.93	0.5965	0.12131	0.5986	-0.1103	0.00291	2.037	1.373	1.689	0.5382	0.571
22.97	0.6382	0.14049	0.6438	-0.1163	0.00159	2.075	1.401	1.708	0.5408	0.573
24.01	0.6838	0.16340	0.6911	-0.1290	-0.00011	2.116	1.430	1.727	0.5424	0.578
25.06	0.7326	0.19000	0.7441	-0.1382	-0.00245	2.172	1.457	1.745	0.5439	0.583
26.10	0.7763	0.21858	0.7933	-0.1453	-0.00506	2.208	1.502	1.784	0.5470	0.589

SYMBOLS

a	linear normal force parameter
A	aspect ratio
c	centre-line chord
C_D	drag coefficient
C_L	lift coefficient
C_m	pitching moment coefficient taken about 0.54 c from wing apex
C_N	normal force coefficient
C_{D_o}	minimum drag of the symmetric wing (= 0.0072)
k	parameter in equation of parabolic envelope of drag polars
K	induced drag factor $= \pi A \dfrac{\left(C_D - C_{D_o}\right)}{C_L^2} = K_1$
	or $= \pi A \dfrac{\left(C_D - C_{D_m}\right)}{\left(C_L - C_{L_m}\right)^2} = K_2$
R	Reynolds number
s	local semi-span
S	wing area
$s(x)$	equation of the leading edge
t	$= \dfrac{K_1}{\pi A}$ - a function of C_L (equation (4))
t_{min}	the minimum value of $t = k$
X	$= \dfrac{K_2}{\pi A}$ - assumed constant for the family of cambered wings (equation (3)
x	chordwise distance from apex in plane of definition
y	spanwise distance from centre-line
z	third axis forming a right handed system of axes with x and y
α	angle of incidence

SYMBOLS (Contd)

Subscripts

DES	the theoretical value of the quantity
α_{DES}	the value of the quantity at the design incidence
m	applicable to the minimum point of the C_D vs. C_L curve of a cambered wing
e	applies to the envelope of the drag polars
c.a.	centre of area
c.p.	centre of pressure
a.c.	aerodynamic centre

REFERENCES

No.	Author(s)	Title, etc.
1	Patricia J. Davies	The design of a series of warped slender wings for subsonic speeds. RAE Technical Report - to be issued
2	C. H. E. Warren	RAE unpublished work 1957
3	D. L. I. Kirkpatrick	Investigation of the normal force characteristics of slender delta wings with various rhombic cross-sections in subsonic conical flow. ARC CP 922 (1965)
4	D. A. Kirby	An experimental investigation of the effect of planform shape on the subsonic longitudinal stability characteristics of slender wings. ARC R & M 3568 (1967)

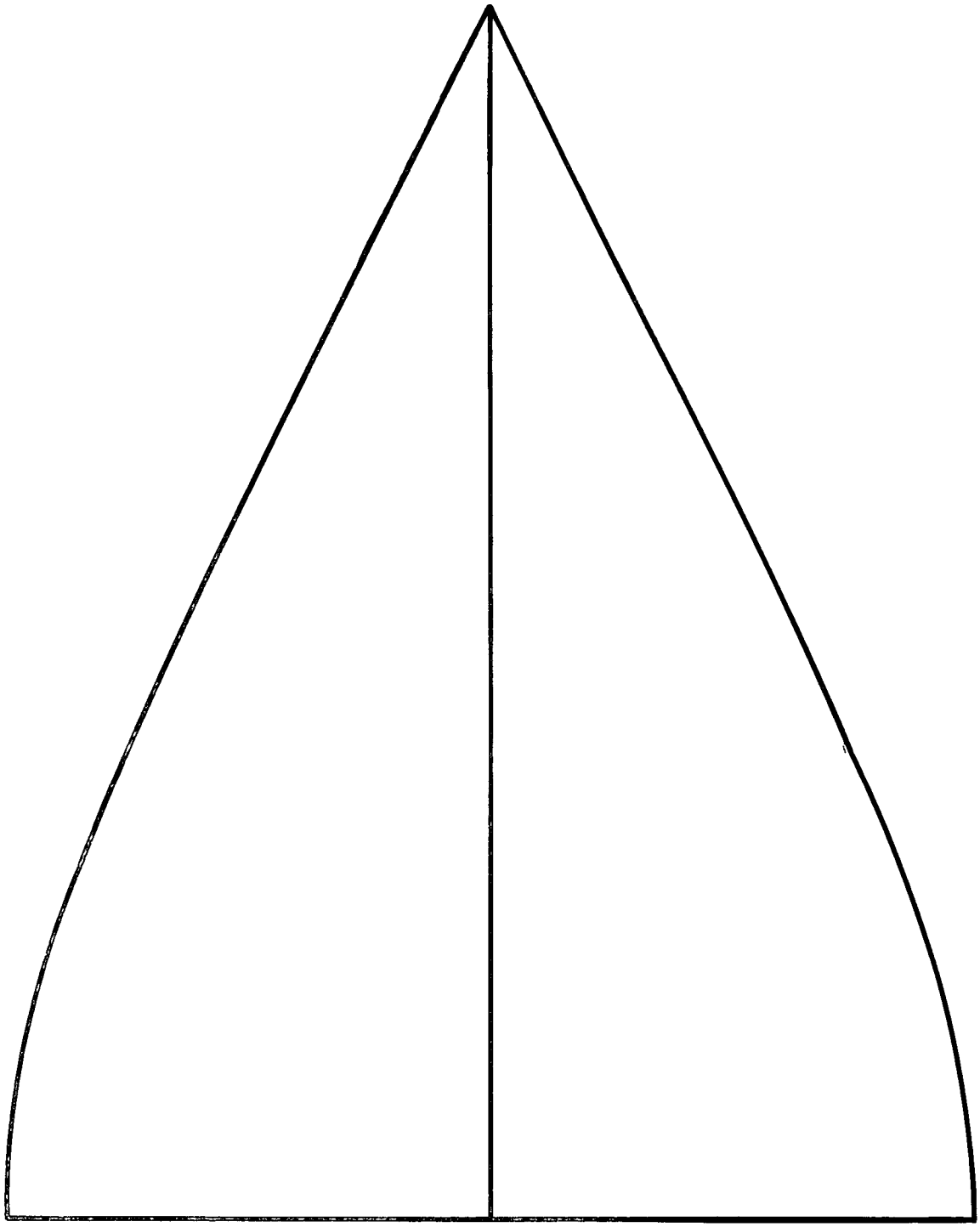

SCALE 2:5

Fig. 1 Mild gothic wing planform

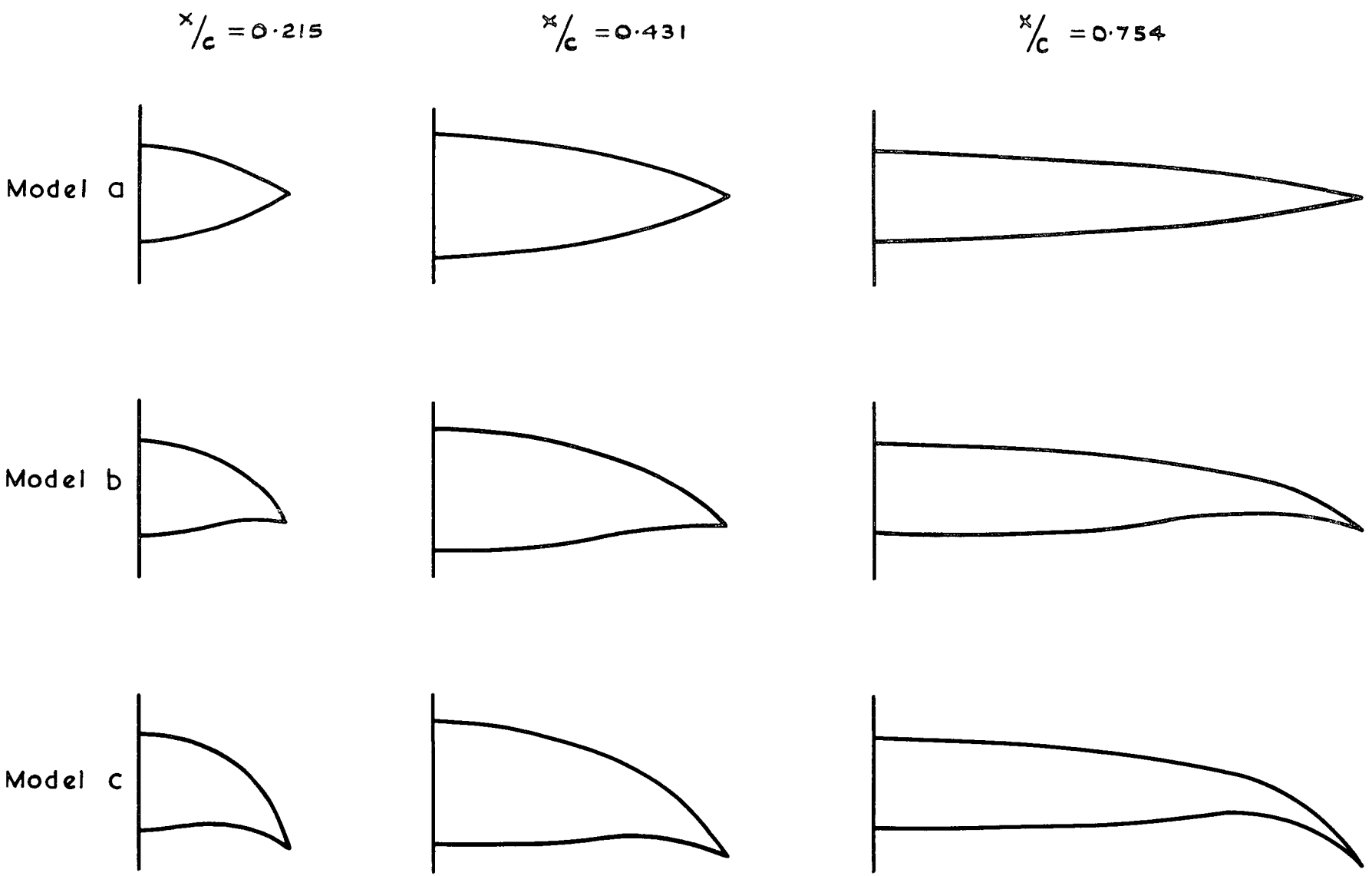

Fig.2 Half scale wing sections of the three models

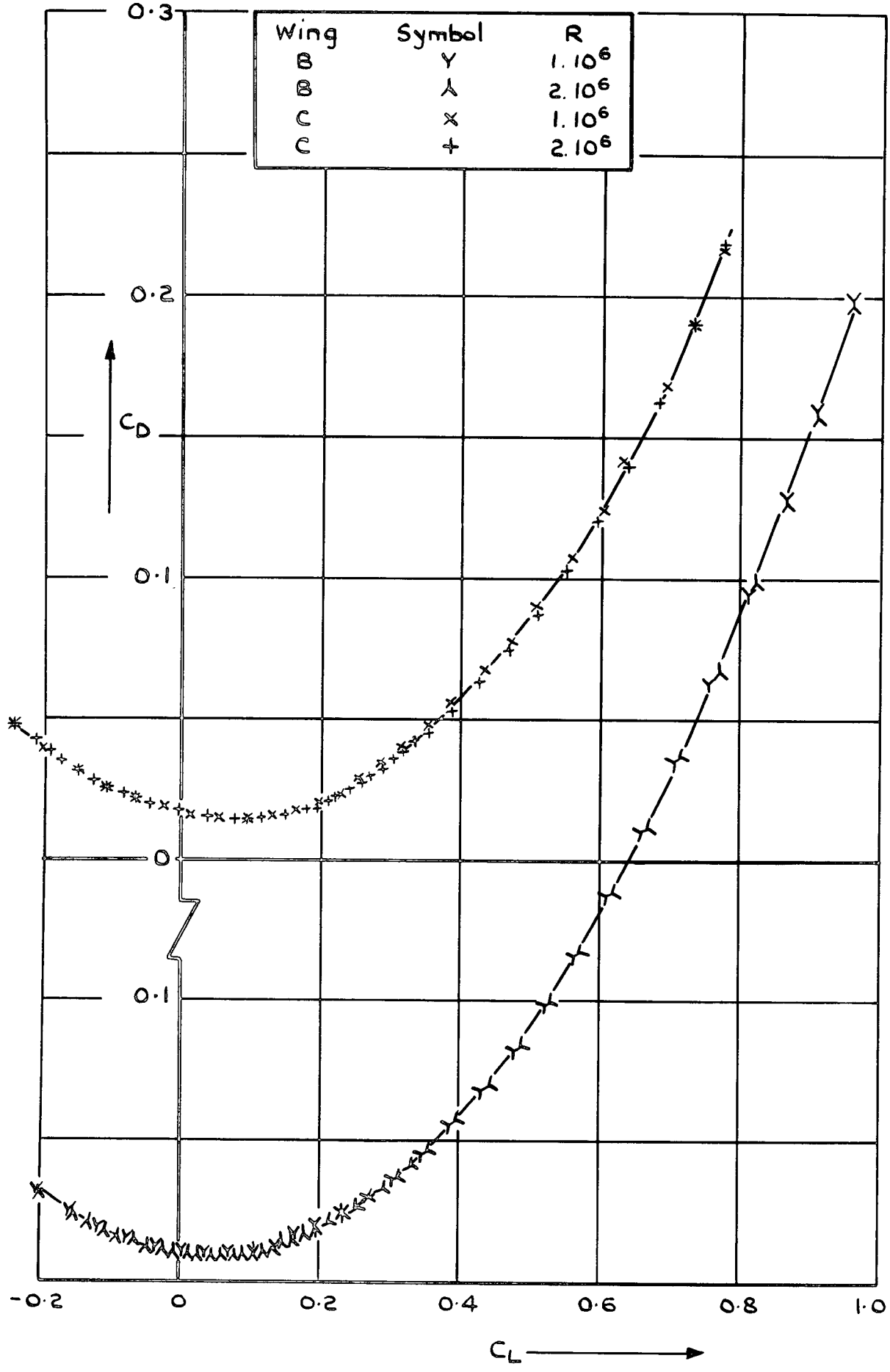

Fig.3 Effect of Reynolds number on the drag polars

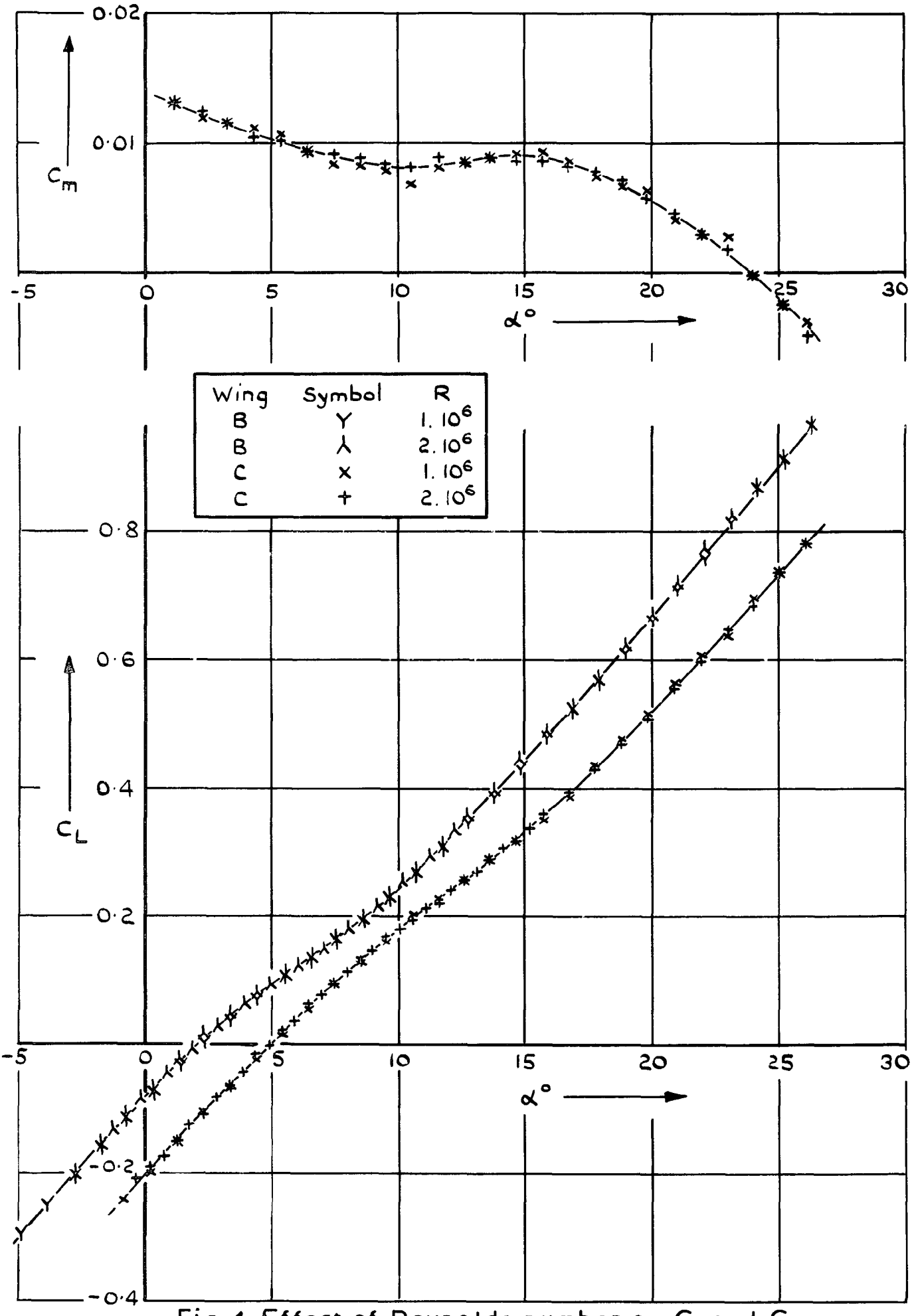

Fig.4 Effect of Reynolds number on C_m and C_L

Fig.5 Attached flow at leading edge of wing C at $\alpha = 10.55°$

Model B. $\alpha = 5.32°$

Model C. $\alpha = 10.55°$

Fig.6 Attached flows on upper surfaces of models B and C. V = 30.5m/s

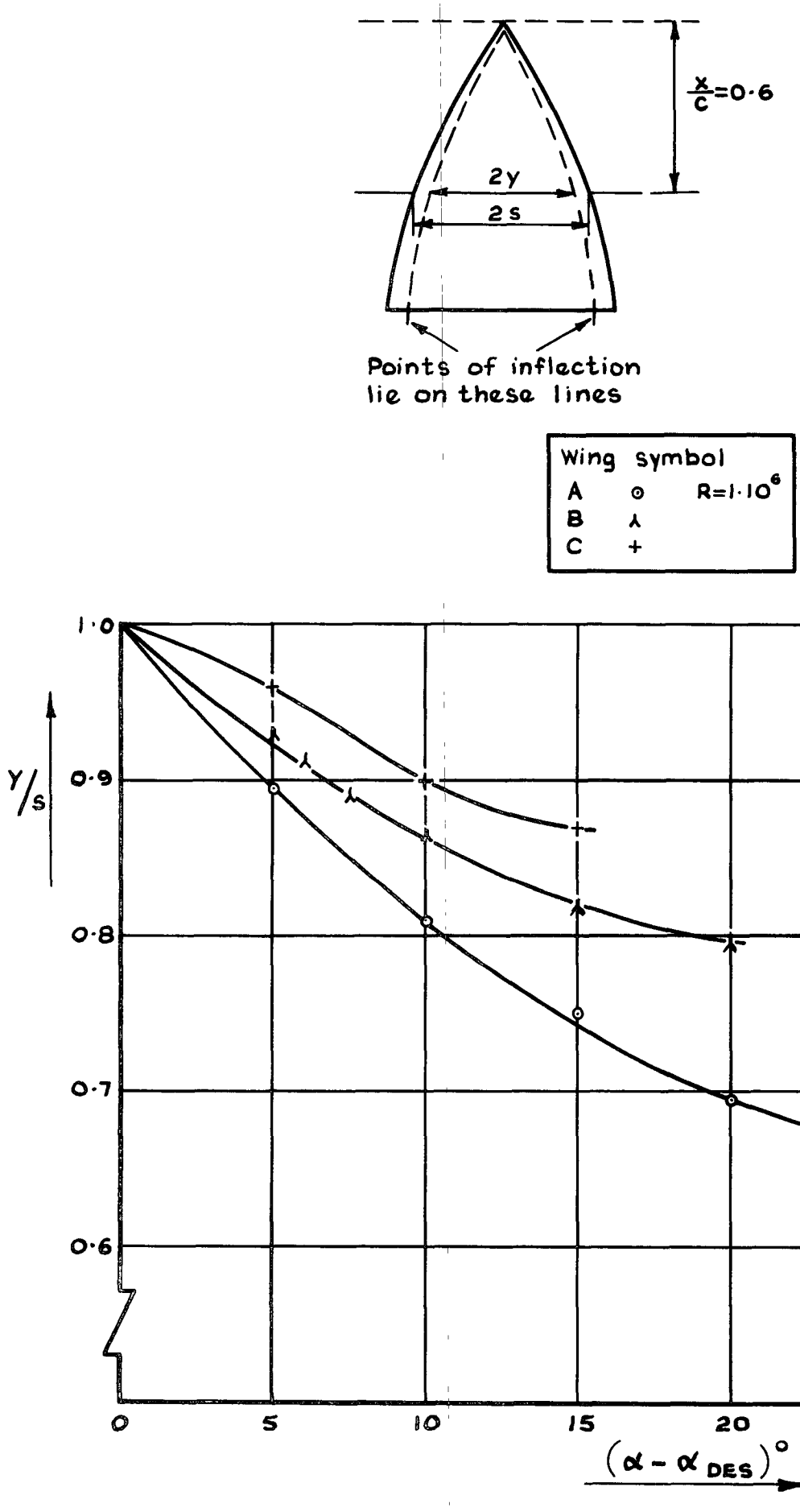

Fig.7 Spanwise position of points of inflection at x/c=0·6

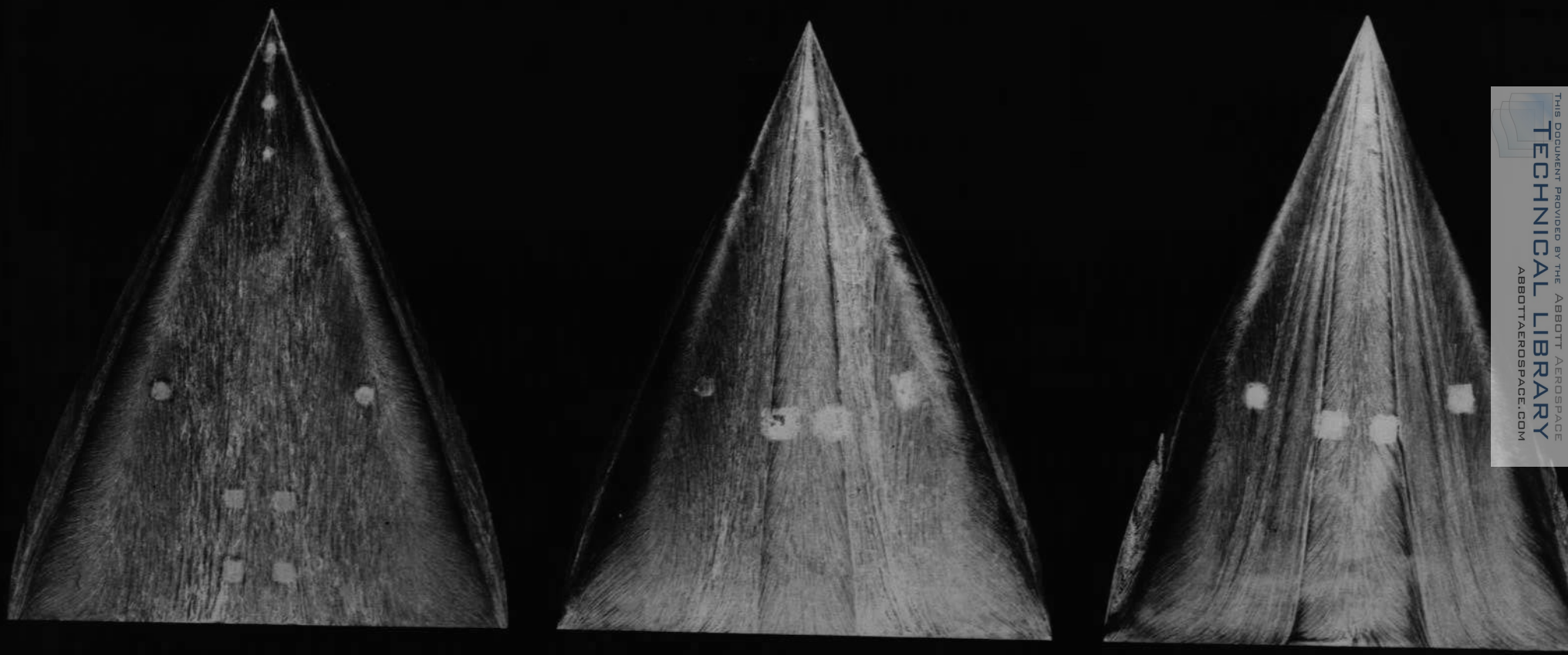

Model A. $\alpha = 15°$

Model B. $\alpha = 20.32°$

Model C. $\alpha = 25.55°$

Fig.9 Flow patterns on upper surfaces of models at V = 30.5 m/sec.,15° above attachment

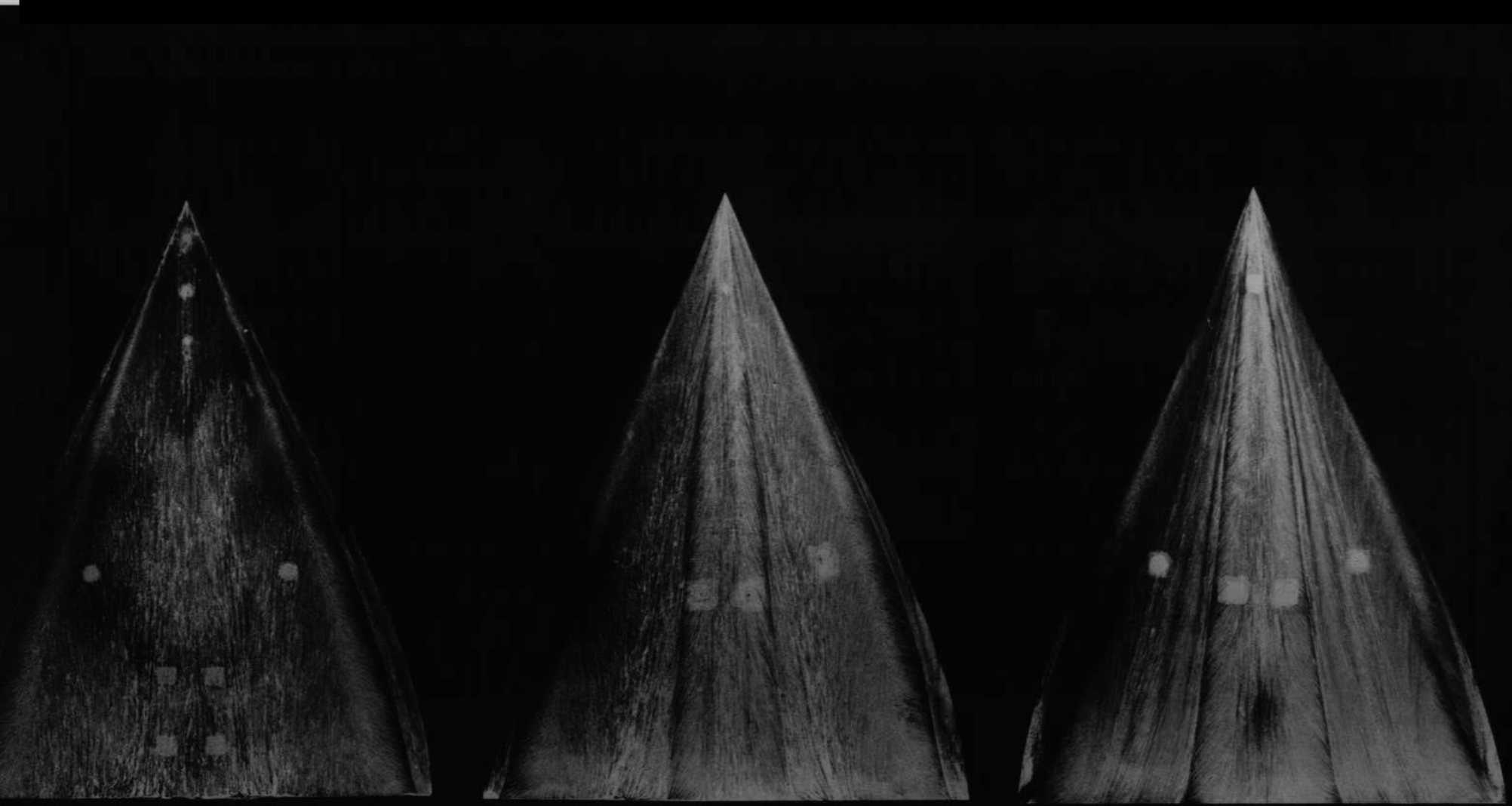

Model A. $\alpha = 10°$ Model B. $\alpha = 15.32°$ Model C. $\alpha = 20.55°$

Fig.8 Flow patterns on upon surfaces of models at V = 30.5 m/sec.,10° above attachment

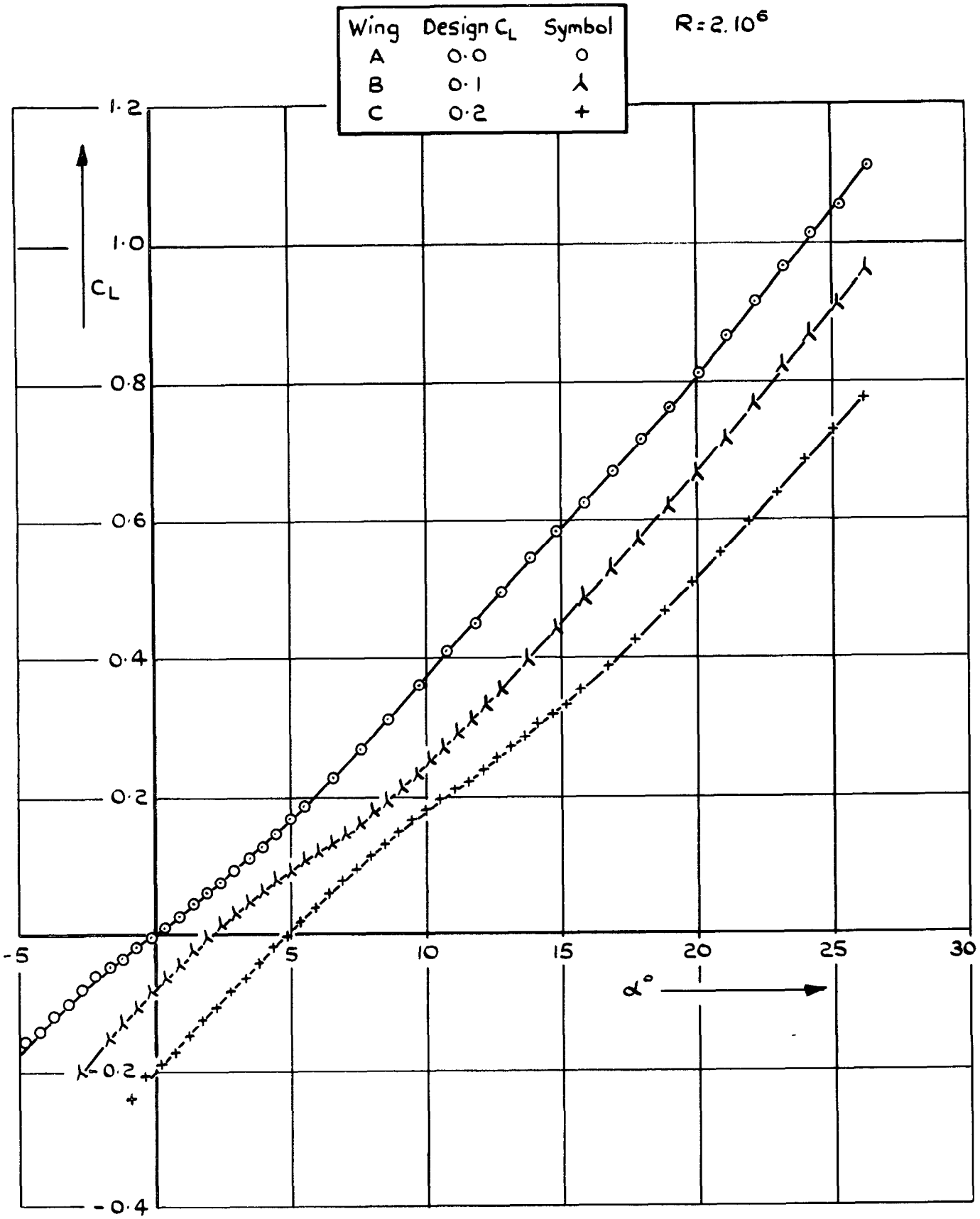

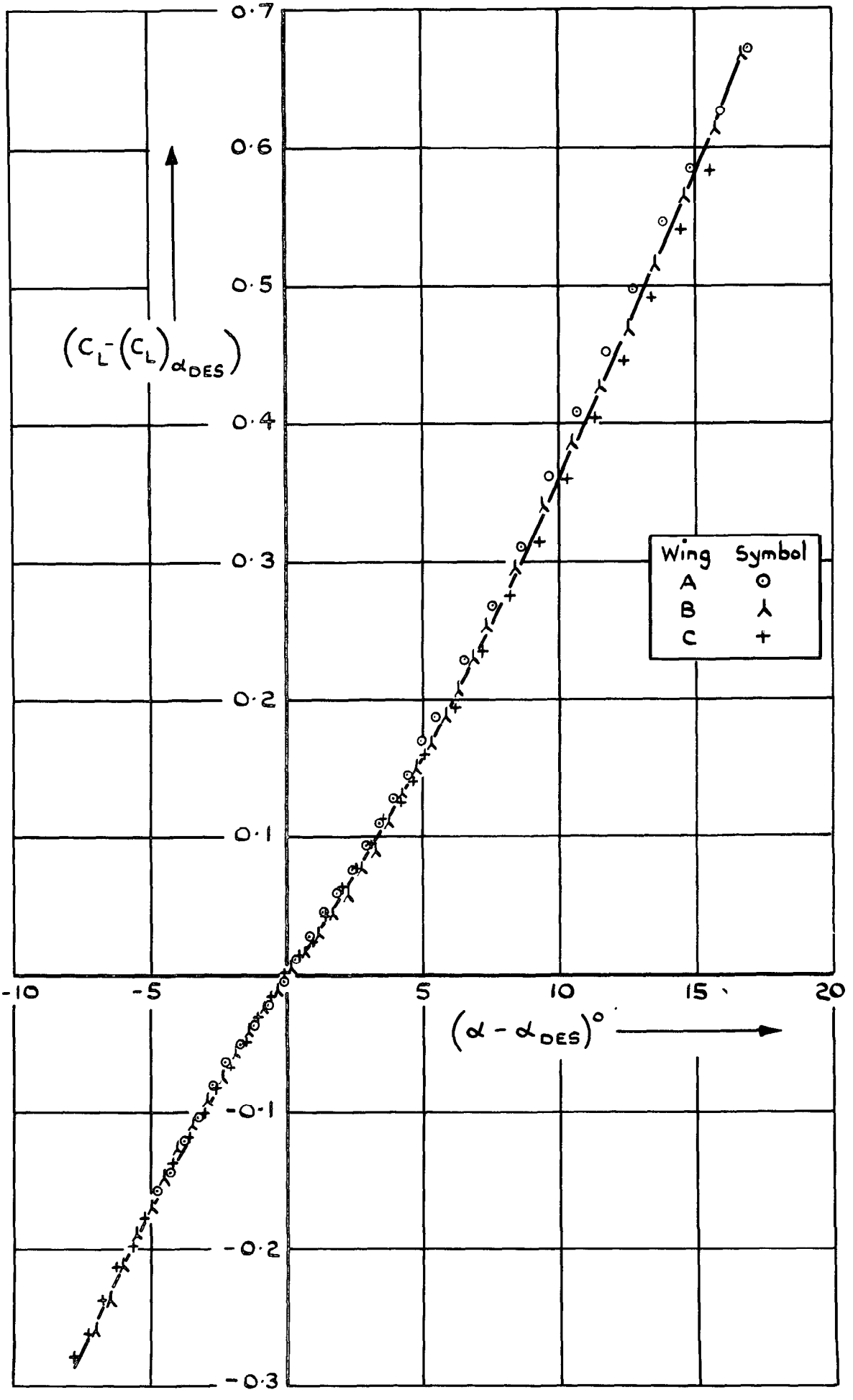

Fig.11 Collapse of lift data

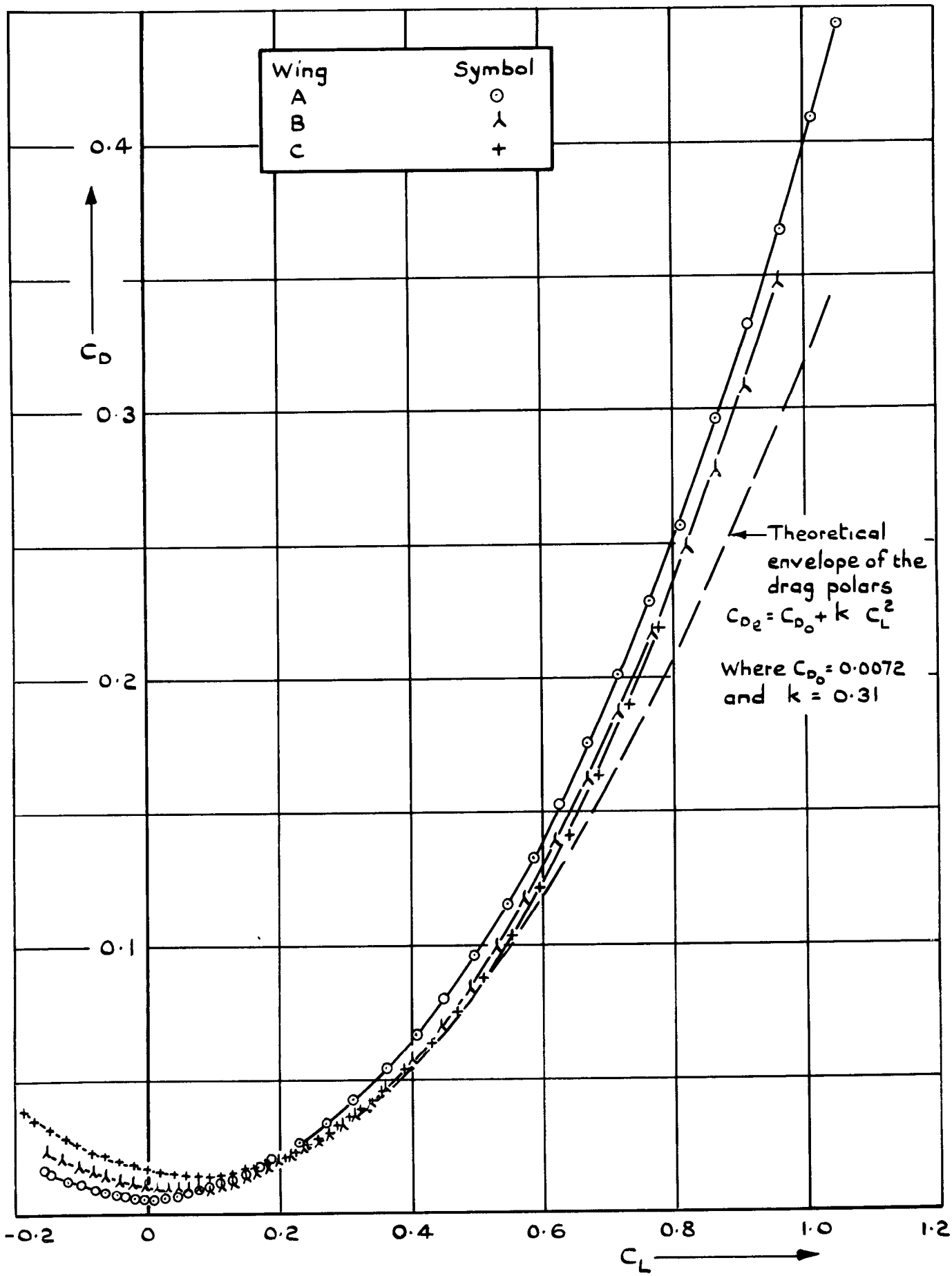

Fig 12 Drag vs lift

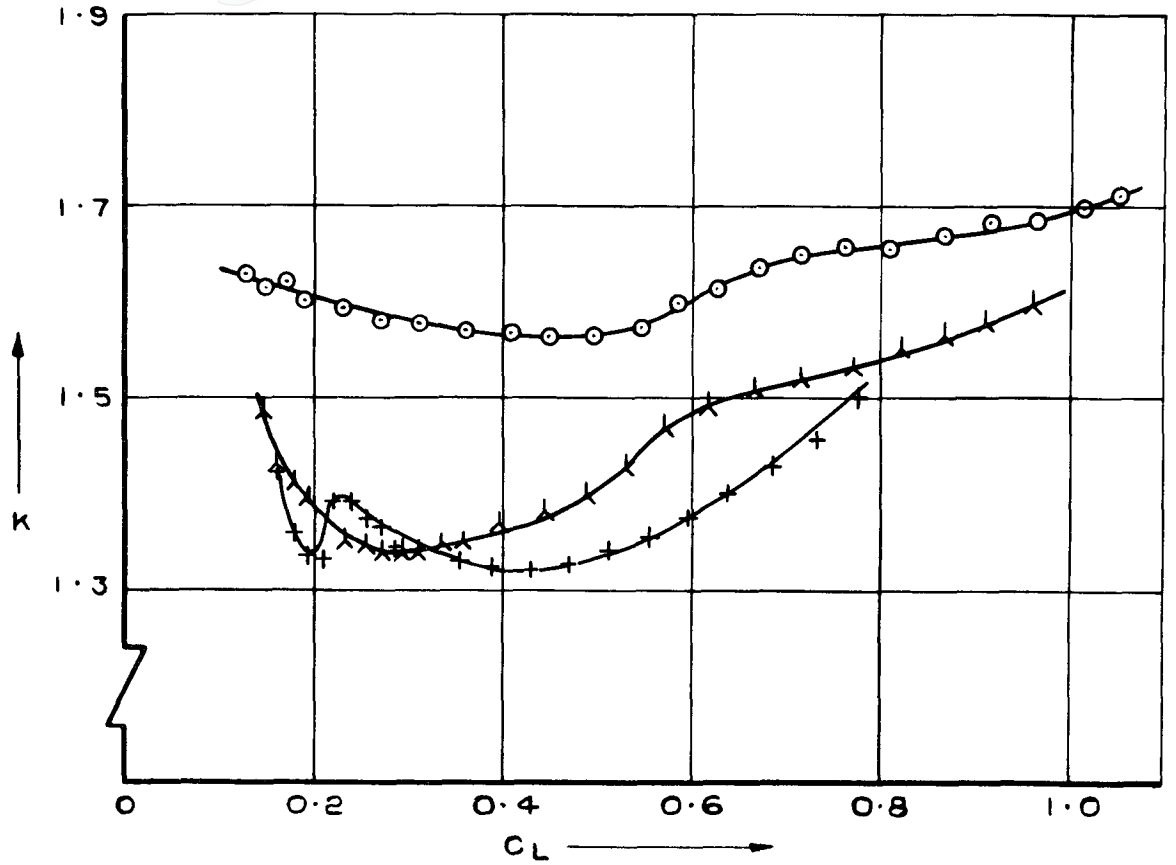

a $K_1 = \pi A (C_D - 0 \cdot 0072) / C_L^2 = t \pi A$ (Eqn 4)

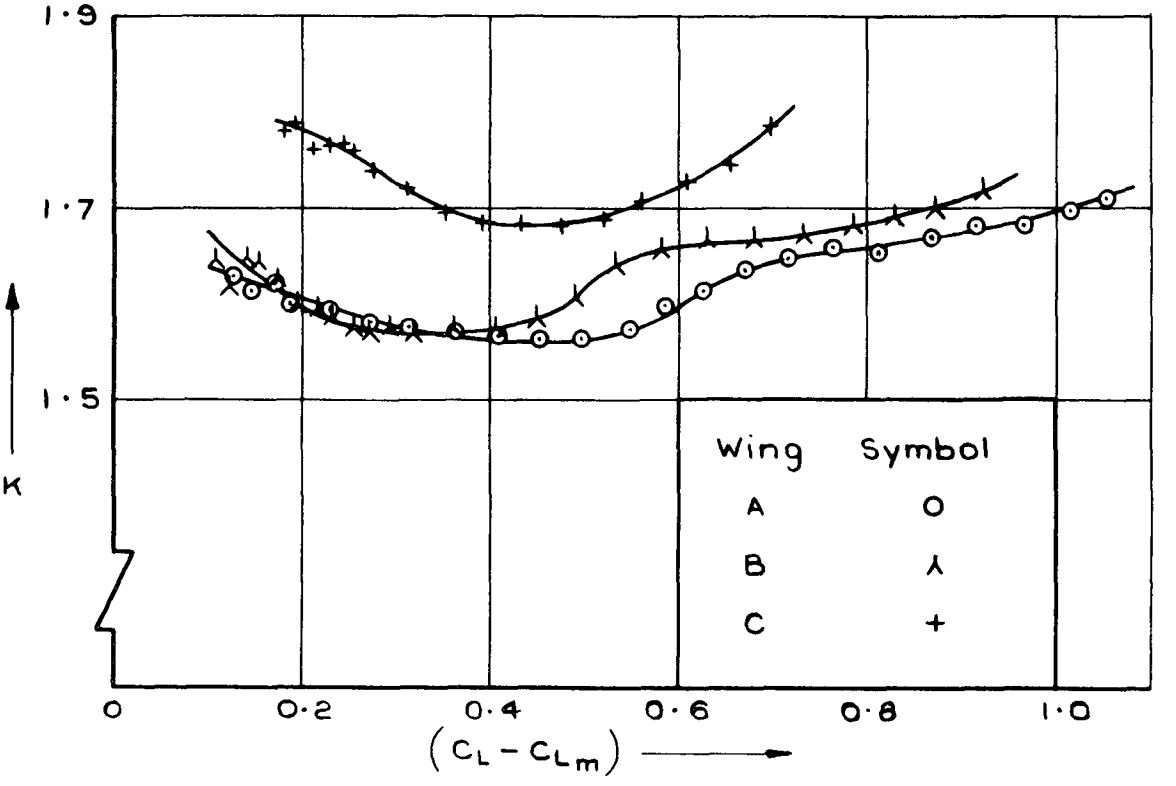

b $K_2 = \pi A (C_D - C_{DM}) / (C_L - C_{LM})^2 = X \pi A$ (Eqn 3)

Fig. 13 a & b Lift – dependent drag factor vs lift

Note: Flagged symbols denote negative values of $(C_L - C_{L_m})$

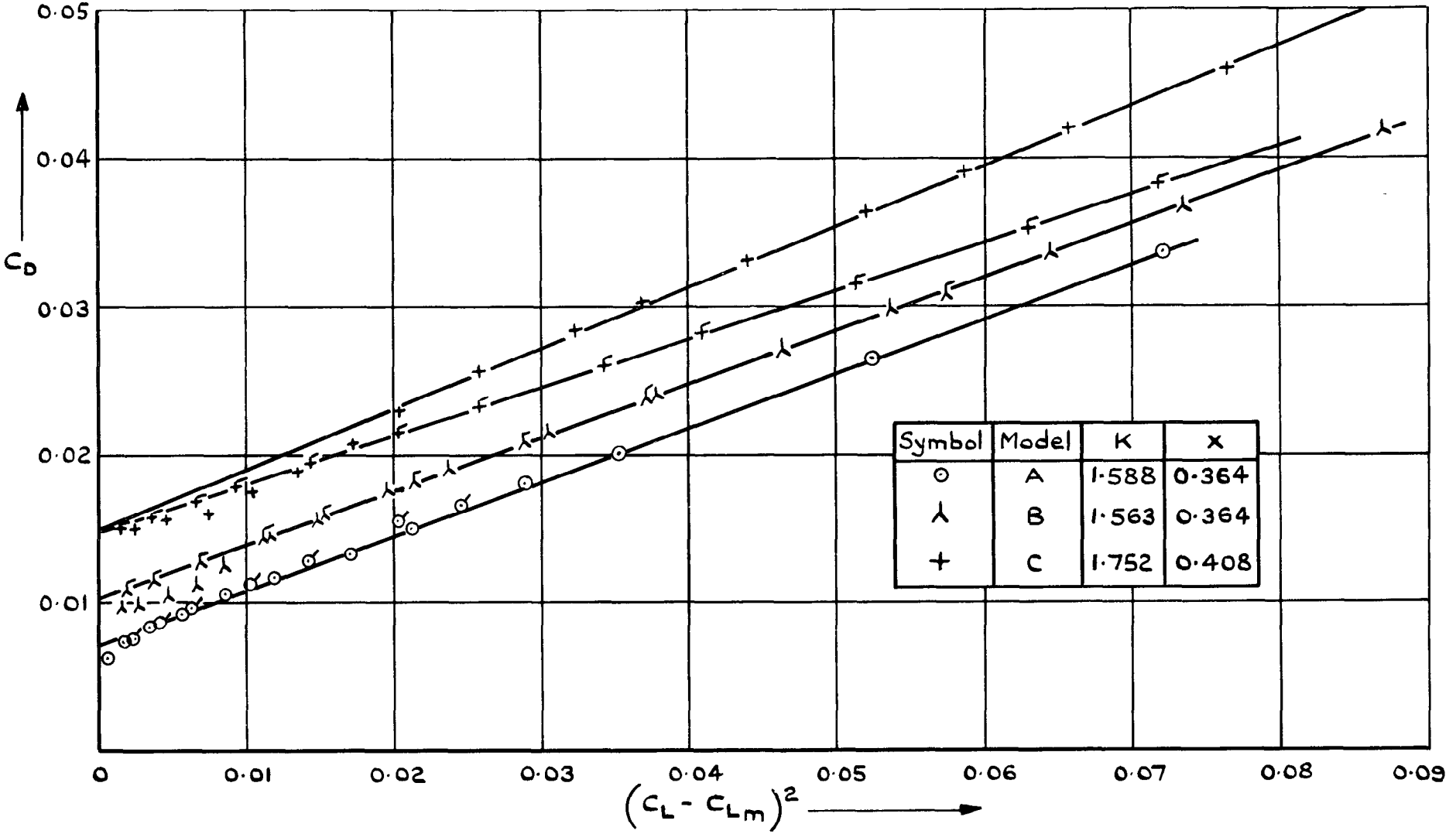

Fig.14 Determination of C_{D_m} and C_{L_m}

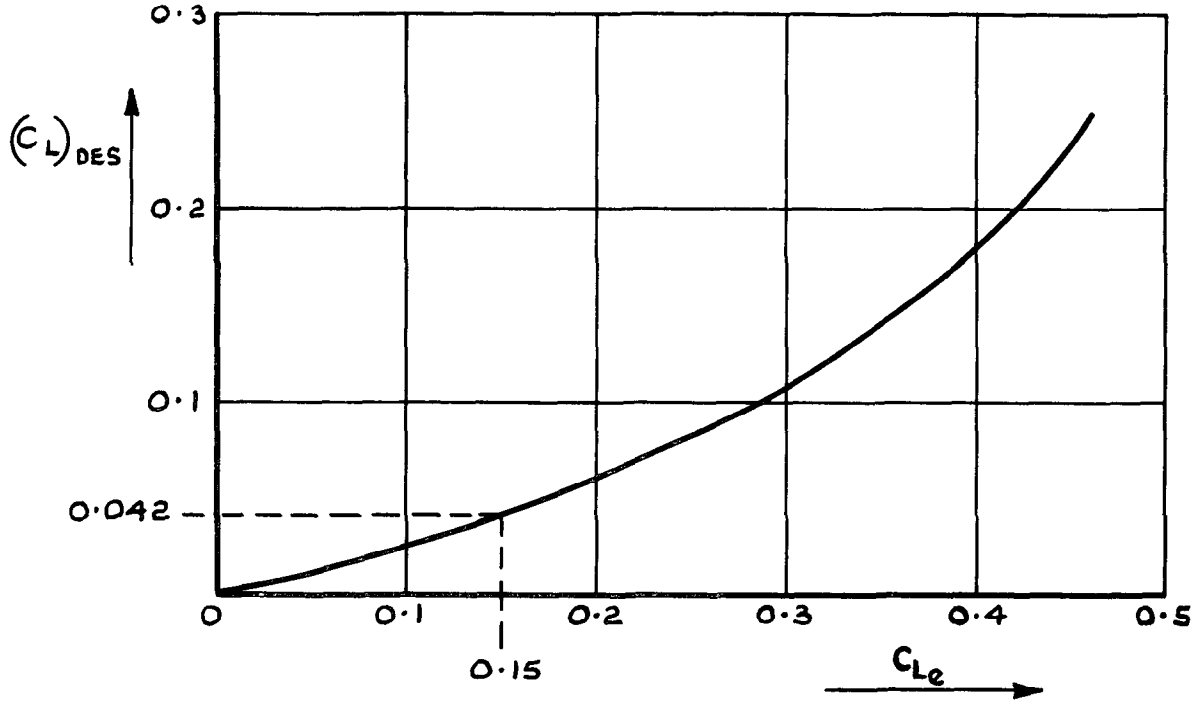

eg The wing which mimises C_D at a C_L of 0·15 should have $(C_L)_{DES} = 0·042$

This wing would have $C_D = 0·0072 + 0·311\,(0·15)^2$
$= 0·0142$ at $C_L = 0·15$

For wings A,B and C at $C_L = 0·15$, $C_D = 0·0157$ for wing A
0·0148 for wing B
0·0157 for wing C

Fig.15 The relationship between $C_{L_{DES}}$ and the C_L at which the drag polars touch the envelope

Note: For the two cambered wings C_N/α is defined by: $\frac{C_N - C_{N\alpha DES}}{\alpha - \alpha_{DES}}$

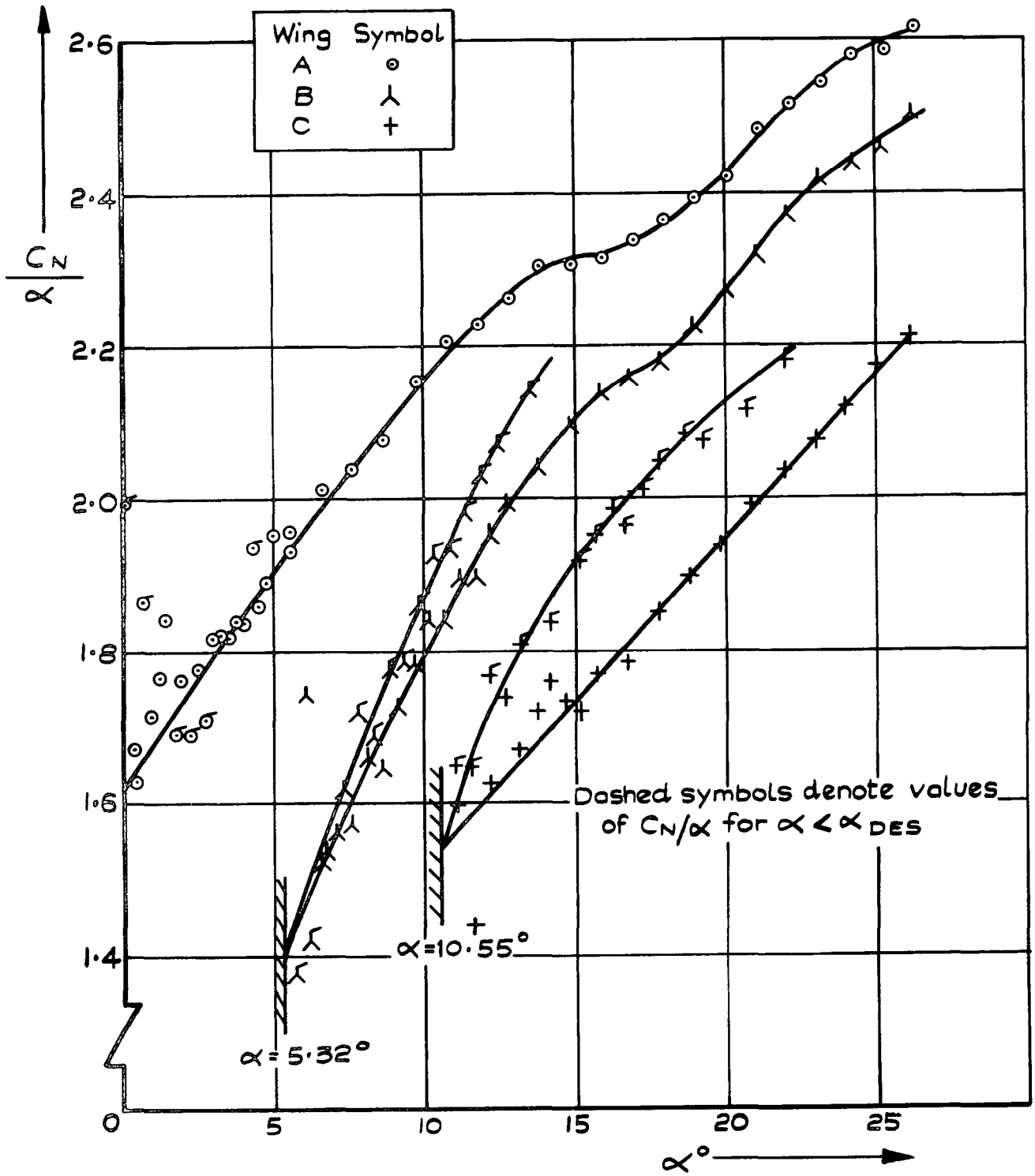

Fig. 16 Effect of camber on normal force

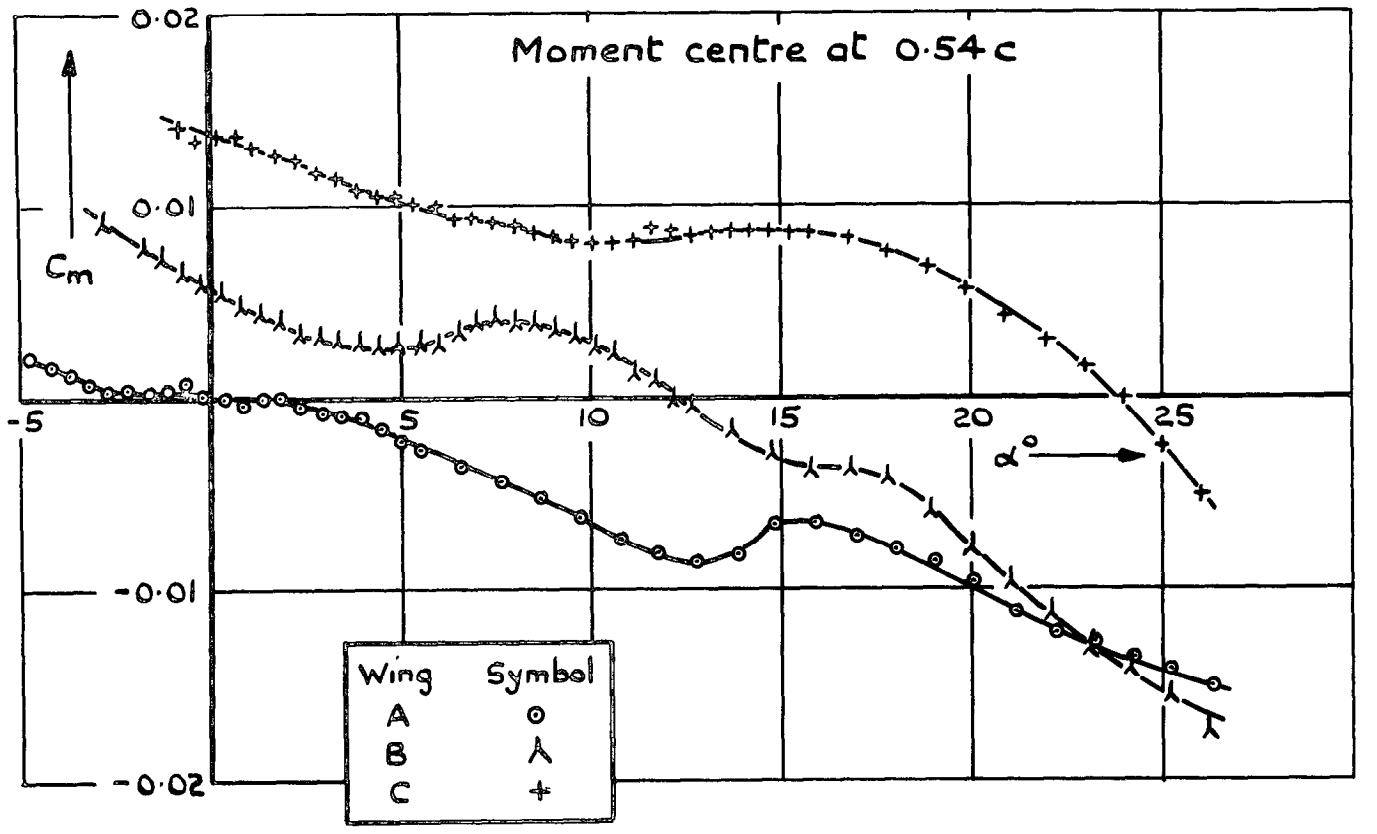

Fig.17 Effect of incidence on pitching moment

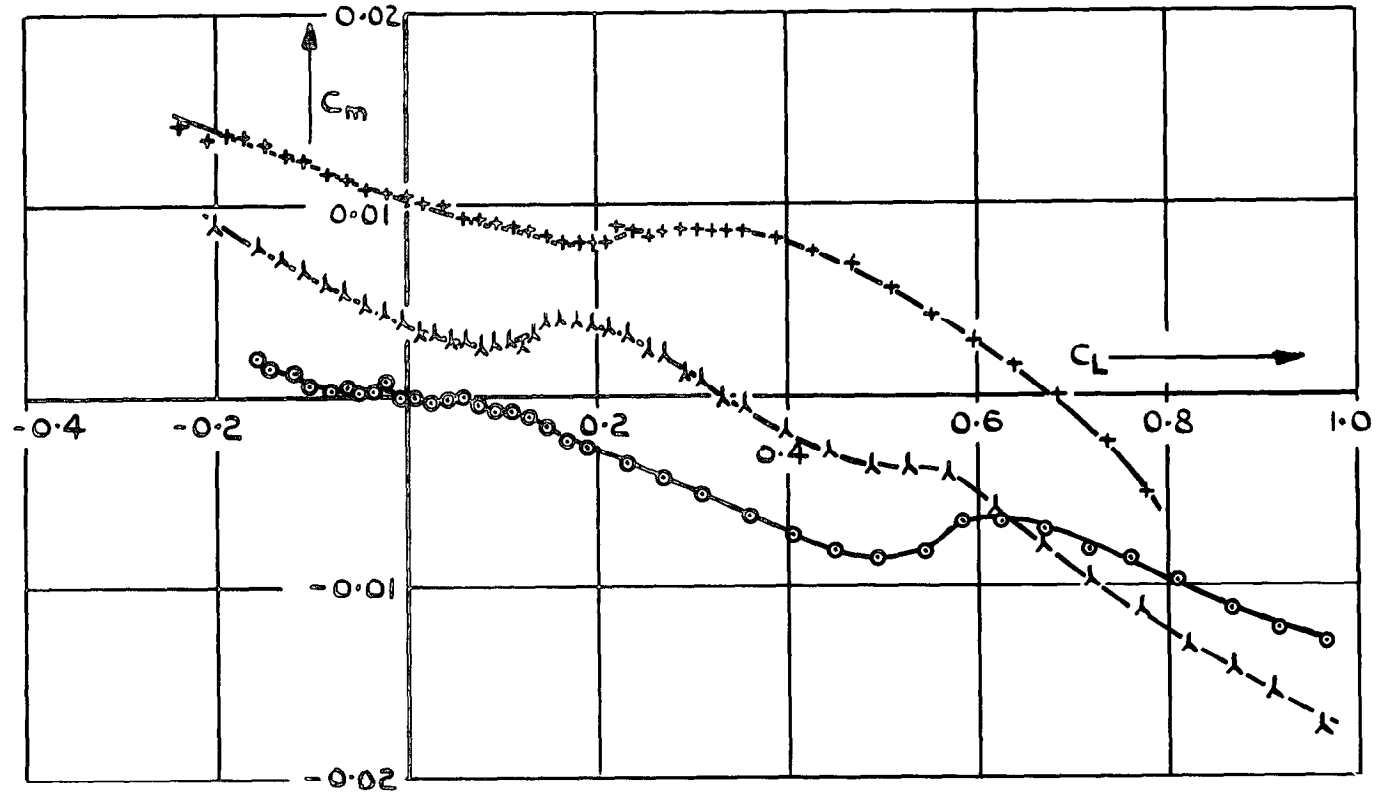

Fig.18 Effect of lift on pitching moment

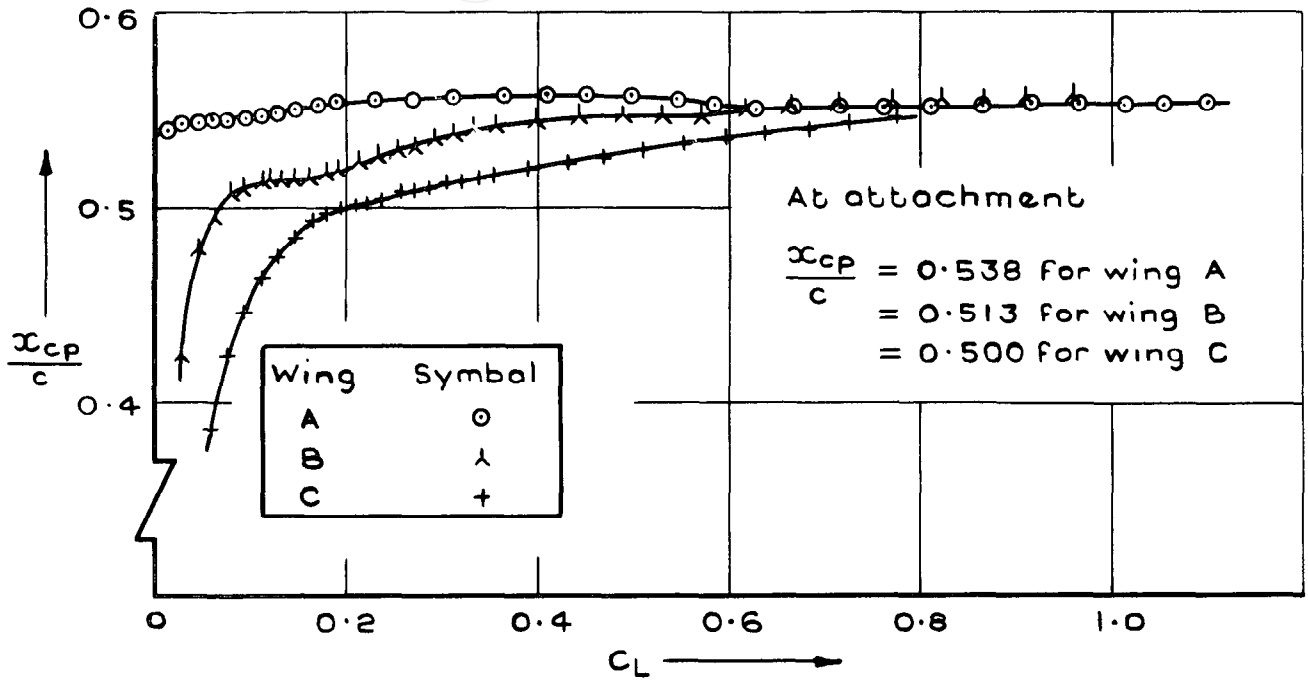

Fig. 19 Position of centre of pressure vs lift

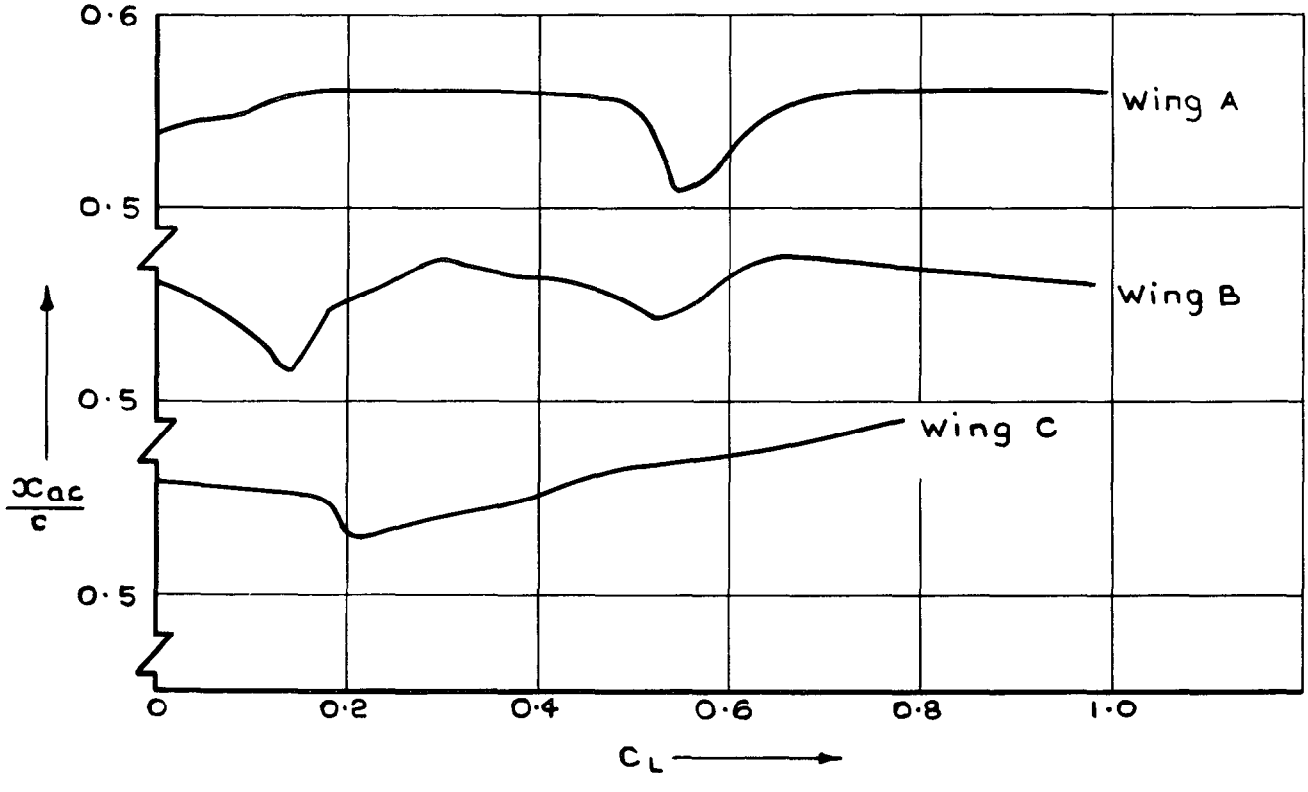

Fig. 20 Position of aerodynamic centre vs lift

DETACHABLE ABSTRACT CARD

A.R.C. C.P. No.1163
October 1970

Butterworth, P. J.

533.693.3 :
533.6.043.1 :
533.6.013.12 :
533.6.013.13 :
533.6.013.152

LOW-SPEED WIND-TUNNEL TESTS ON A FAMILY OF CAMBERED WINGS OF MILD GOTHIC PLANFORM OF ASPECT RATIO 1.4

The longitudinal characteristics of a family of one symmetrical and two cambered mild gothic wings of aspect ratio 1.4 and thickness-to-chord ratio of 0.09 were investigated and the results are presented with analysis. The two cambered wings were designed to have attached leading edge flow at lift coefficients of 0.1 and 0.2 respectively, at a specified angle of incidence. The force measurements and flow visualisation show that the design criteria have in fact been satisfied though additional inboard shoulder separations near the apex were observed under certain conditions.

A.R.C. C.P. No.1163
October 1970

Butterworth, P. J.

533.693.3 :
533.6.043.1 :
533.6.013.12 :
533.6.013.13 :
533.6.013.152

LOW-SPEED WIND-TUNNEL TESTS ON A FAMILY OF CAMBERED WINGS OF MILD GOTHIC PLANFORM OF ASPECT RATIO 1.4

The longitudinal characteristics of a family of one symmetrical and two cambered mild gothic wings of aspect ratio 1.4 and thickness-to-chord ratio of 0.09 were investigated and the results are presented with analysis. The two cambered wings were designed to have attached leading edge flow at lift coefficients of 0.1 and 0.2 respectively, at a specified angle of incidence. The force measurements and flow visualisation show that the design criteria have in fact been satisfied though additional inboard shoulder separations near the apex were observed under certain conditions.

Published by
HER MAJESTY'S STATIONERY OFFICE

To be purchased from
49 High Holborn, London WC1 V 6HB
13a Castle Street, Edinburgh EH2 3AR
109 St Mary Street, Cardiff CF1 1JW
Brazennose Street, Manchester M60 8AS
50 Fairfax Street, Bristol BS1 3DE
258 Broad Street, Birmingham B1 2HE
80 Chichester Street, Belfast BT1 4JY
or through booksellers

C.P. No. 1163

SBN 11 470431 7